Comprehensive analysis of the local seismic response in the complex Bšuyšukczekmece landslide area (Turkey) by engineering-geological and numerical modelling

Celine Bourdeau, Luca Lenti, Salvatore Martino, O Oguz, E Yalcinkaya, P Bigarre, S Coccia

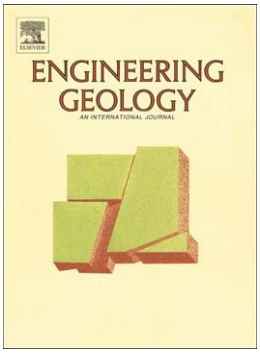

Comprehensive analysis of the local seismic response in the complex Büyükçekmece landslide area (Turkey) by engineering-geological and numerical modelling

C. Bourdeau, L. Lenti, S. Martino, O. Oguz, E. Yalcinkaya, P. Bigarrè, S. Coccia

PII: S0013-7952(17)30024-8
DOI: doi:10.1016/j.enggeo.2017.01.005
Reference: ENGEO 4456

To appear in: *Engineering Geology*

Received date: 5 July 2016
Revised date: 27 December 2016
Accepted date: 5 January 2017

Please cite this article as: Bourdeau, C., Lenti, L., Martino, S., Oguz, O., Yalcinkaya, E., Bigarrè, P., Coccia, S., Comprehensive analysis of the local seismic response in the complex Büyükçekmece landslide area (Turkey) by engineering-geological and numerical modelling, *Engineering Geology* (2017), doi:10.1016/j.enggeo.2017.01.005

Comprehensive analysis of the local seismic response in the complex Büyükçekmece landslide area (Turkey) by engineering-geological and numerical modelling

Bourdeau C.[a], Lenti L.[a], Martino S.[b*], Oguz O.[c], Yalcinkaya E.[c], Bigarrè P.[d], Coccia S.[d]

[a] Institut Français des Sciences et Technologies des Transports, de l'Aménagement et des Réseaux (IFSTTAR-Paris) 14-20 Boulevard Newton Cité Descartes Champs sur Marne F-77447 Marne la Vallée Cedex 2, France
[b] Dpt. Scienze della Terra and Centro di Ricerca per i Rischi Geologici (CERI), Università di Roma, "Sapienza", P.le Aldo Moro 5, 00185 Roma, Italy
[c] Istanbul University, Engineering Faculty, Geophysical Engineering, Avcilar, Istanbul, TURKEY
[d] INERIS Ecole des Mines des Nancy Campus ARTEM CS 14234 F-54042 Nancy Cedex France

[*] Corresponding Author

ABSTRACT

Multi-risk management requires a strong comprehension of possible effects induced by natural hazardous events. In this regard, landslides triggering due to earthquakes results from complex interactions between seismic waves and slopes. Multidisciplinary approaches can significantly contribute to better understand such interactions. The large Büyükçekmece landslide (about 1500 m wide and 1830 m long) located in Turkey (Avcilar peninsula), about 15 km northward from the North Anatolian Fault Zone (NAFZ), was selected as case-study in the framework of the European project "*MARSite – Marmara Supersite: new directions in seismic hazard assessment through focused Earth observation in the Marmara Supersite*". The Avcilar area was recently affected by the 17th August 1999 Mw 7.4 Kocaeli and by the 12th November Mw 7.2 Düzce earthquakes. The Büyükçekmece landslide involves upper Oligocene to lower Miocene deposits, consisting of silty clays, tuffs and sands. No

earthquake-induced re-activations are testified so far but the landslide area was interested by a very intense urbanization during the last decade. A detailed engineering-geological model for the local seismic response of the Büyükçekmece landslide slope was constructed based on geophysical measurements, data from a multisensor in-hole monitoring system and stress-strain numerical modeling. Several tens of earthquakes were recorded from October 2014 to May 2015 in the landslide site by considering in-hole and surface data. The reliability of the local seismic response obtained by numerical modelling respect to the empirically derived one was checked in terms of both site-to-reference spectral ratios and transfer function between surface and downhole sites inside the landslide mass. The 2D numerical amplification functions confirm that the local seismic response is a consequence of the complex geological setting of the landslide slope while no relevant amplification effects can be referred to topographic features. Based on these results, the interaction between seismic waves and the Büyükçekmece landslide slope cannot be neglected to evaluate the possibility of future landslide re-activations.

Keywords

Landslide, engineering-geological model, local seismic response, numerical modeling

1. INTRODUCTION

Local seismic amplification can favor landslide (re)activations also in unexpected far field conditions (Delgado et al., 2011) so increasing the natural hazard. Landslide areas are often characterized by complex geological setting due to the displacements caused by the landslide mechanisms which significantly modify the original slope setting, introducing dislodged blocks and stratigraphic irregularities. In this regard, multidisciplinary approaches can be regarded as particularly suitable to analyse the local seismic response in landslide areas, including engineering-geological modelling, geophysical investigations and numerical modelling.

Earthquake-induced landslides represent a big concern in seismic risk management since severe damage and losses were recently caused by co-seismic slope failures. As reported by Bird and Bommer (2004) the greatest damage caused by earthquakes is often related to landslides (Petley 2012). According to the World Bank report (Dilley et al., 2005), 3.7×10^6 km^2 of land surface is prone to landslides worldwide, and nearly 300 million people live in areas exposed to potential landslide risk. A spatio-temporal distribution of deadly landslides, was recently presented by Haque et al. (2016) for 27 European countries over the last 20 years (1995–2014); this distribution shows that catastrophic landslides are widely distributed throughout Europe, however, with a great concentration in mountainous areas. The average economic loss per year in Europe due to landslides is approximately 4.7 billion Euros.

As it regards the earthquake-induced landslide, the behavior of slopes during earthquake shaking as well as the induced landslide mobility depend on their complex interactions with seismic waves. Such interactions are controlled by several features among which the slope geometry, the landslide mass properties and the physical characteristics of the seismic waves (Lenti and Martino, 2013). Stress-strain numerical modeling performed under dynamic conditions helps a better understanding of the aforementioned interactions; these models rely on very strong constraints to reproduce the engineering-geological setting of the slope and to restitute reliable outputs in terms of amplification functions or induced displacements (Martino, 2015).

In the context of the prediction of earthquake-induced movements of landslides, possible interactions between seismic waves and slopes have been analysed in several studies (Del Gaudio and Wasowski, 2007; Bourdeau and Havenith, 2008; Danneels et al., 2008; Lenti and Martino 2012, 2013) to describe how the triggering conditions depend on seismic input properties such as energy, frequency content, directivity and peak ground acceleration (PGA), as well as on the slope topography and geological setting. Some case studies (Bozzano *et al.*, 2008, 2011; Alfaro et al., 2012; Delgado et al., 2015) pointed out the role of seismic input vs. landslide mass interactions for justifying local amplification effects. In particular, it was already highlighted (Delgado et al., 2011) that pre-existing large landslides can represent outliers with respect to the predictive curves proposed by Keefer (1984) and Rodriguez et al. (1999), as they can interact with far-field earthquakes characterized by long-period spectral contents.

In the framework of the European Project "*MARSite – Marmara Supersite: new directions in seismic hazard assessment through focused Earth observation in the Marmara Supersite*" a case study was selected 35 km West of Istanbul, in the Avcilar-Beylikdüzü peninsula, about 15 km North from the seismogenetic North Anatolian Fault Zone (NAFZ, see Fig. 1). This area is of particular interest for the assessment of landslide susceptibility to earthquake triggering as: i) several rototranslational landslides prone to earthquake-induced reactivation are inventoried (Lenti et al., 2016), with width ranging from 250 up to 1000 m, length varying between 300 and 1850 m and maximum depth of sliding surface ranging from some tens of meters up to 100 m; ii) it was recently affected by the 17th August 1999 Mw 7.4 Kocaeli and by the 12th November Mw 7.2 Düzce earthquakes. The Büyükçecmece landslide (Fig.2), with a volume of about 50 Mm^3, is the biggest one surveyed in the Avcilar-Beylikdüzü peninsula; the continuous landslide movement is causing damages to several buildings, roads and infrastructures.

The paper begins by illustrating the case-study and the engineering-geological model reconstructed so far. In the following, the collected seismic records are introduced and used to validate numerical models of the local seismic response in the landslide area. The obtained results are discussed along selected cross sections, whose traces are longitudinal and transversal respect to the landslide mass, to output the main effects due to the stratigraphic setting of the slope as well as to the presence of the dislodged landslide mass.

2. THE BÜYÜKÇEKMECE LANDSLIDE

Geomorphological evidence from remote sensing and field studies allowed to identify and map characteristic landforms of a rototranslational mechanism in the Büyükçekmece landslide slope: these landforms include a main scarp, several secondary scarps, several landslide terraces (characterized by evident counter slopes, sometimes responsible for the presence of water pools). Two earth flows, the first one located along the left side of the landslide mass and the second one at its toe (Fig.2b), were also surveyed. The collected observations of damage to roads, buildings, walls, and infrastructures helped to contour the landslide mass, but do not provide elements to infer the first time failure of the slope. Based on these evidences, the landslide can be regarded as active, even though earthquake-induced reactivations of the Büyükçekmece landslide are unknown so far; nevertheless, the very recent urbanization of the area does not allow to exclude past undocumented reactivations. More in particular, the Büyükçekmece landslide is a complex phenomenon (according to the classification by Varnes 1978) that includes a rototranslational landslide combined to earth-flows; besides, it is still an active landslide with a retrogressive behavior.

2.1 Geological and geomorphological setting of the landslide

The Büyükçekmece landslide is approximately 1830 m long and it can be divided into eight blocks of different sizes, with an average width of about 130 m. Each block is lowered and bordered by secondary failure surfaces and scarps; the blocks are counter-slope tilted and the angle of tilting varies gradually from 30° up to 40° moving downslope. Such a setting points out the repeated reactivations of the landslide and its retrogressive evolution.

The geological setting of the Büyükçekmece landslide area was defined according to previous studies (Dalgiç 2004). In the Avcilar-Beylikdüzü peninsula the Paleozoic basement is composed of Devonian limestones belonging to the Trakya and to the Dolayoba Formations which are overlaid by Oligocene to upper Miocene sedimentary rocks (Fig. 3).

These deposits can be divided into three main units: the Danisment Formation (upper Oligocene) consisting of stiff clays and claystone-shales containing loose sand horizons and tuff levels of different thicknesses (Fig.3a,b); the Kiraç member of the Istanbul Formation (upper Oligocene - lower Miocene) consisting of sands and gravels belonging to fluvial deposits generally poorly or not cemented (Fig.3c) with rare interbeds of tuff; the Bakirköy member of the Çekmece Formation (upper Miocene) consisting of alternating calcarenites, marls and clay layers (Fig.3d). The Oligocene-Miocene deposits show an almost horizontal attitude with dip angles generally lower than 10°.

Manmade fills with average thicknesses of about 2 m widely cover the sedimentary deposits due to the intense and recent urbanization of the area. According to Sen (2007), the structural setting of the Avcilar-Beylikdüzü peninsula is characterized by two fault systems. The first one is NW-SE oriented and dislodges the Danisment Formation; the age of the fault system is probably pre-Upper Miocene as it does not cut the Upper Miocene deposits. The second fault system is NNW-SSE to WNW-ESE oriented and cuts the deposits of the Çekmece Formation. The Büyükçekmece landslide mass mainly involves the Danisment Formation and the Kiraç member of the Istanbul Formation while the Bakirköy member of the Çekmece Formation is partially involved in the detachment area (Fig.2a). The dislodgement produced by the

landslide movement caused a lowering of the Kiraç member up to 50 m respect to the outcropping stable area.

2.2 Reconstruction of the landslide geometry and slope geology

The reconstruction of the landslide geometry and geology to perform numerical simulations relies on several geomorphological evidences as listed above and the processing of geophysical measurements as described in this paragraph.

A "preliminary model" of the landslide mass and of its dislodged portions (named "blocks" in the following) along one longitudinal cross section and four transversal cross sections of the site was first created (Fig.4). The definition of the abovementioned cross section takes into account the geometries of the scarps, the measured dip of the outcropping strata and a geometrical feedback consisting of a reversal of the present landforms to reconstruct the original (i.e. prior to any landsliding process) shape of the slope. Although each cross-section is by definition two-dimensional, considering the longitudinal as well as several transversal cross sections provides a general overview of the three-dimensional setting of the landslide.

In order to strengthen the reliability of this preliminary model, starting from the end of May 2014, geophysical investigations were carried out on site consisting of (Fig.2b): 5 vertical electrical sounding profiles (VES); 19 seismic noise measurements (NM); 20 seismic refraction microtremor (ReMi) profiles with MASW; 1 borehole drilled on July 2014 until 70 m b.g.l. in the frame of the MARsite project; 3 accelerometric stations, corresponding to the location of FM, SU and FO stations shown in Figs.2b, 4. In addition, several boreholes log stratigraphies were made available by the Municipality of Istanbul in the framework of the

project. The detailed results of these investigations, including the reconstruction of 3D geometry of the landslide mass based on multiphysics and log-stratigraphic data correlations, were published by Yalcinkaya et al. (2016).

Geophysical measurements and geological field surveys in the landslide area were combined to obtain a more comprehensive engineering-geological model of the site. Based on the collected evidences, 5 geological cross-sections were reconstructed in the landslide mass area (1 longitudinal cross section L and 4 transversal cross sections T1, T2, T3 and T4, see Fig. 4). To this aim, each measurement site within a reliable buffer was mapped and projected along the cross sections; following this approach, measurements that were located too far from the cross section were not considered.

In more detail, the following criteria were used to transpose the geophysical data along the engineering-geological cross sections:

- the seismic refraction lines and the MASW were considered to establish variations of Vs (i.e. dynamic stiffness) with depth and to project the so derived seismo-stratigraphic logs along the geological cross sections;

- the noise measurements were considered to check the consistency of the geological layering with possible resonance frequencies;

- the VES resistivity logs were projected along the geological cross sections to compare the resistivity values with the subsoil layering;

- available boreholes log stratigraphies were considered including the one drilled for the MARSite project (located at point 3 in Fig.2b).

The analysis of seismic refraction data (Yalcincaya et al., 2016) allowed to reconstruct the subsurface geology up to 20 m. In the uppermost layer (up to 5 m below the ground level) P-wave velocities are very low, in the order of 300-400 m/s, but they locally sharply increase probably depending on the location of the water table. Regarding S-wave velocity profiles, derived from MASW and ReMi measurements, the penetration depth for MASW measurements is about 30 m, while it reaches about 80 m for ReMi measurements. Although a sharp velocity increase could be expected below the landslide mass, no such obvious impedance contrast was obtained but an almost gradual increase of velocity up to 600 m/s with depth and a minimum superficial value of about 150 m/s were observed. Single-station seismic noise measurements were performed at 32 sites using GURALP CMG-6T velocimeter sensors with a natural frequency of 1Hz, using 50 min long time-windows.

Data were processed (Yalcincaya et al., 2016) using the horizontal to vertical spectral ratios (HVSR) technique to derive the resonance frequencies. Results show that only few stations have clear first resonance peak generally close to 1Hz and other peaks within a wider frequency range from 4 to 6 Hz.

Based on the engineering-geological model of the slope such a finding can be attributed to a limited impedance contrast along the sliding surface between the landslide mass and the substratum, which are mostly composed by the same geological formation, partially remolded and destructured in the landslide mass. The performed noise measurements pointed out

anthropic vibrations (focused at about 1.5Hz) that could alter data interpretation as they interfere with the natural resonance. As discussed by Yalcincaya et al. (2016), neglecting the anthropic peaks in the HVSR analysis since they do not show polarization, the obtained curves indicate that the landslide area is characterised by higher resonance frequencies (generally ≥2Hz) than the sites located outside from the landslide area. Considering an average Vs of 400 m/s and a resonance of 2 Hz, the landslide mass should have a thickness of about 50 m. Such an evidence of seismic resonance related to landslide mass overlying a stiffer bedrock was already collected in other case studies by different authors (e.g. Méric et al., 2007; Bozzano et al., 2008; Coccia et al., 2010; Bozzano et al., 2011; Delgado et al., 2015; Martino et al., 2016).

VES measurements were performed at 4 points (see Fig.3 for location). The resistivity values measured within the landslide mass are generally lower than 20 ohm·m. A typical obtained VES profile shows a sharp increase of the resistivity values up to 100 ohm·m at almost 65 m depth below the ground level that can be related to the sliding surface. The lowest resistivity values (of almost 10 ohm·m) generally can be related to the sandy deposits belonging to the Kiraç member of the Istanbul Formation.

As shown by the reconstructed final engineering-geological model of the site the main sliding surface is located up to 55 m b.g.l. as confirmed by the log stratigraphy of the borehole drilled in the framework of the MARSite project (see point FM of Fig.2b for location). Based on the reconstructed engineering-geological model, a total volume of about 50 million cubic meters is assessed for the landslide. Moreover, based on the available geophysical data as well as on

field observations, a ground water circulation through the landslide mass is assumed; the most consistent hypothesis about the local hydraulic conditions is that both the Kiraç sandy deposits and the debris , which covers the old secondary scarps, host the most surficial aquifer generating local pools and pound areas, mainly concentrated along the uphill block edges.

2.3 Monitoring system of the landslide

A multiparametric monitoring system was installed in the Büyükçekmece landslide at the end of October 2014 with the aim of detecting possible triggers of landslide movement as well as of increasing the rate of displacement measurements in time. In this regard, occurrence and intensity of destabilizing actions (i.e. water pore pressures, rainfalls and earthquakes) as well as displacements inside and outside the landslide mass were continuously recorded and made visible in real time by a web-monitoring system. The monitoring system consists of: a GPS-RTK system, based on the state of the art technologies of differential GPS, a seismometric system and a geotechnical system. The GPS station is designed for periodic 3D displacement measurements with a precision up to a couple of centimeters. The GPS system is composed of: 1 reference GPS station, located upslope on the upper roof of a “Shopping center” (SC) in a stable zone (see Fig.3 for the location of this station); 2 measurement stations, installed in the landslide area: so-called “Farm” (FM) and “House” (HS) (see Fig.3 for the location of these stations).

The seismometric system (described in more details in paragraph 3.1) consists in two 3D seismic probes (installed close to the FM station at -45m in a 70 meters deep borehole – FO -

and on the surface - SU) to measure seismic ground motions (sensor type 2Hz GEOSPACE, bandwidth ±3dB, inherent sensibility 2 V/in/s) sampling at 1kHz with a threshold at 1μm/s.

The geotechnical system includes: 2 piezometers (vibrating wire technology) installed at FM station measuring pore pressures at different depths (-36m and -51m b.g.l.) in the MARSite borehole with a measuring range of 0-200 kPa; 1 moisture sensor, installed at FM station horizontally at about 30 cm depth; 1 rainfall meter and a temperature sensor installed at HS station.

Digital raw data are collected by a SYTGEM-vlp acquisition unit, which was also installed at FM station. The GPS system recorded continuous displacements of the landslide mass in the WE downslope direction with an average rate of almost 2 cm/month (Fig. 5). Based on this result and according to the velocity scale proposed by Cruden and Varnes (1996), the Büyükçekmece landslide can be classified as a very slow phenomenon.

Measurements collected by the seismometric system consist in 65 earthquake records and a continuous record of meteorological and piezometric data from November 2014 until May 2015. The recorded earthquakes have PGA values ranging from 10^{-2} to 10^{-5} m/s^2, corresponding to magnitudes from 1.5 up to 6.1 and epicentral distances varying from 15 km up to 550 km.

The geotechnical recorded data show a groundwater circulation related to two different circuits at location FM: the first one perched in the sandy deposits of the Kiraç member (corresponding to a pore pressure ranging between 29 and 32 kPa) and the second one perched in the landslide mass debris above the sliding surface (corresponding to a pore

pressure ranging from 36 and 42 kPa). A preliminary correlation analysis indicates that a seasonal trend exists in the pore water pressures recorded at the -51m piezometer while a more irregular trend characterizes the -36m piezometer which seems mostly related to intense rainfalls.

Anomalies in comparison to the aforementioned trends correspond to spurious data recorded by the deeper piezometer only; nevertheless, these anomalies occurred in correspondence to higher displacement rates recorded for the WE component of the landslide movement by the GPS monitoring system at station FM. Comparing other monitored quantities (Fig. 5), no relationship can be easily deduced between pore pressures (u), displacements (resulting from cumulative GPS measurements) and shaking energy of recorded earthquakes (reported as cumulative AI). Fig 5 also shows the values of mm/hour pore pressure rates (u(t)) at -51m and -36m (6 hour filtered) as well as the cumulative rainfall intensities.

3. LOCAL SEISMIC RESPONSE OF THE LANDSLIDE

Due to the very close location of the NAFZ and to the very intense urbanization development in the landslide area during the last decade, characterizing the local seismic response of the landslide is useful for the assessment of possible earthquake-induced reactivation of the Büyükçekmece landslide. Empirical and numerical site-to-reference spectral ratios as well as transfer functions between surface and downhole sites inside the landslide mass were calculated. In the following, the procedure adopted for analyzing empirical and numerical data is described in more detail.

3.1 Seismic recordings

The seismometric system installed in the MARSite borehole, namely at the SU and at the FO stations, recorded 88 earthquakes since October 2014 and until May 2015. Among these records, 45 were also collected by the permanent velocimetric station (TEPT). Their characteristics and locations are reported in Table 1. Only these records were considered to assess the local seismic response of the Büyükçekmece landslide in terms of amplification functions as well as to define the transfer function associated to the 3-components seismic stations installed in the MARSite borehole.

A data processing was performed on the earthquakes records to derive the distributions of Arias Intensity (AI) vs PGA values as well as the distribution of earthquakes characteristic periods (T_m, as defined by Bray and Rathje, 1998) vs. AI. The obtained results are reported on Fig.6 for SU, FO and TEPT stations considering the two horizontal components separately. The resulting distributions demonstrate that a strong correlation exists between energy and kinematic earthquake parameters in the landslide site. Moreover, the surface stations SU and TEPT show higher values for both PGA and AI respect to the in-hole station FO. The T_m distribution reveals that the computed values generally vary in the range 0 - 0.2s.

Since TEPT station is located outside from the landslide area, it was considered as a reference for computing site-to-reference spectral ratios (SSR) (*sensu* Borcherdt, 1994). We checked that the mean horizontal/vertical spectral ratio (HVSR) for TEPT station (Field and Jacob, 1995) does not exceed significantly 2 (Fig.7a) in the frequency range of interest (0 – 20Hz). To this aim, the time histories were cut to isolate the earthquakes from the rest of the signals

and all the considered signals were rotated to derive the movement along the principal direction of sliding of the landslide (E-W) and along the orthogonal direction (N-S). The signals were band-pass filtered between 0.1Hz-40Hz to avoid the effects of long-period terms (removing of drifts) due to the instrumental response of the sensors (Butterworth 4 poles and 2 passages) and Fast Fourier Transforms (FFTs) were computed for each recording. The FFTs were smoothed considering a frequency window of 0.5 Hz and the HVSRs were computed considering separately the two horizontal components (N-S and W-E oriented). The results obtained for the NS and WE components were then arithmetically averaged and mean values and standard deviations of HVSRs for all the recordings were finally computed.

The SSR functions at the borehole station (SU/TEPT) were computed considering all the recorded ground motion components (Fig.7b). Empirical transfer functions which characterize the soil column of the landslide mass at the MARSite borehole site were also assessed considering the records at SU and FO stations. To compute these transfer functions, the acceleration time histories were cut to isolate earthquakes from the rest of the seismic signals and all the signals were rotated to deduce the movement along the principal sliding direction of the landslide (almost E-W oriented) and along the normal direction (N-S). The procedure adopted for filtering, smoothing and averaging FFTs was the same as for HVSRs. The spectral ratios SU/FO were computed for each ground motion direction (i.e., N-S, W-E and Z) and mean and standard deviation were computed for the SU/FO spectral ratios (Fig. 8a and c).

3.2 Numerical modeling

To assess the local seismic response of the Büyükçekmece landslide in terms of seismic amplification and wave propagation pattern along the slope surface and to define possible relations with the geological setting of the slope and its topography, numerical simulations were undertaken on the longitudinal (L) and on the four transversal (T1, T2, T3 and T4) cross sections of the landslide by the 2D finite difference code FLAC 7.0 (Itasca 2011). An homogeneous slope model was also created for the longitudinal cross section L in order to shed light on the parameters controlling the spatial variations of ground-motion amplifications along the slope surface, i.e. pointing out possible effects due to the slope topography. Below is a description of the main steps of the numerical modeling for the longitudinal cross-section. A similar procedure was adopted for the other transversal cross-sections (T1, T2, T3 and T4). The parameters used for the modeling are reported in Table 2. The landslide area was discretized into square meshes allowing an accurate representation of wave transmission through the model up to 10 Hz (Kuhlemeyer and Lysmer, 1973). Based on the materials properties (in particular the minimum shear-wave velocity Vs) and the frequency content of the input motions (in particular the maximum frequencies), in the main zone of interest (i.e. inside the landslide mass), the element size is approximately 2-3 m, resulting in a total number of nodes equal to 800 * 134 (along x and y direction, respectively) for the longitudinal section L, 534 * 134 (along x and y direction, respectively) for the transversal cross-sections T1 and T2, 575 * 134 for the transversal cross-section T3 and 400 * 100 for the transversal cross-section T4. Absorbing quiet boundaries (Kuhlemeyer and Lysmer, 1973) and free field boundaries (Cundall et al., 1980) were applied along the base of the model and the lateral boundaries respectively to prevent the reflection of outward propagating waves

back into the model. A linear visco-elastic model was applied to all materials. Energy dissipation in the soil was solved using a Rayleigh damping function, a commonly used method to provide damping that is approximately frequency-independent over a restricted range of frequencies (Itasca, 2011). A critical damping ratio (also known as the fraction of critical damping) equal to 2% was used in the landslide zones of the numerical domain and 0.5% elsewhere (i.e., in the substratum).

A first order Ricker wavelet (i.e. Gabor function, Semblat and Pecker, 2009) containing main frequencies in the range 0.1 to 10 Hz was applied in the form of a vertically upward propagating SV stress wave (Fig. 9a). Signal duration is 10 s but only the first 0.15 s are characterized by non-null values. To prevent numerical errors during the dynamic calculation, this input record was checked for baseline drift: indeed, we checked that no continuing residual velocity or displacement existed after the motion had finished. This input was selected to validate the model: in particular, the propagation of the seismic signal inside and along the surface of the model was analyzed to check that no spurious reflections come back into the model from the quiet boundaries, and the numerical transfer and amplification functions were assessed and compared with the empirical ones.

Three earthquakes among the 45 recorded earthquakes at TEPT reference station were also selected to perform numerical simulations (earthquakes EQ22, EQ33 and EQ37 of Table 1). They were chosen because their locations are along the NAFZ at different distances from the landslide site (10, 50 and 100 km) and their spectra (shown on Figure 6) lay in the statistically significant range of all the FFTs computed for the 45 recorded earthquakes. These signals

were applied to the base of the longitudinal section in the form of in-plane and vertically upward propagating SV stress wave (Fig. 9b, c, d) to compare the so derived amplification functions with the one obtained using the Ricker wavelet. To prevent numerical errors during the dynamic calculation, these inputs were also checked for baseline drift: indeed, we checked that no continuing residual displacements neither inertial velocity existed after the motions had finished. These signals were band-pass filtered between 0.1-10 Hz to take into account numerical limitations due to the mesh properties of the model.

4. RESULTS

The reliability of the local seismic response modelled by FLAC code was checked comparing the empirical SSRs (SU/TEPT) and the transfer function (SU/FO) obtained at the MARSite borehole from the 45 recorded earthquakes, with the same functions obtained through numerical modelling (Fig.8). To this aim, the numerical outputs obtained using the Ricker signal and the three selected earthquakes were averaged among 3 consecutive grid-nodes close to SU location along the L section (i.e. along a 6 m extended surface zone) and among 3 consecutive grid-nodes close to the FO position within the MARSite borehole (i.e. i.e. along a 6 m extended vertical zone).

Nevertheless, before evaluating the reliability of the modelled seismic response the efficiency of the assumed boundary conditions was also checked for all the modelled cross-sections by analyzing the propagation patterns of displacements along the surface (Figs. 10-15). The wave

propagation plots show that using as input the first order Ricker wavelet no spurious reflections of waves come back from the boundaries of the models.

The results obtained in terms of SSRs (SU/TEPT) (Fig. 8b) show an acceptable fit in terms of both frequency peaks and amplification amplitudes (if the standard deviations are considered). More in particular, Fig. 8b shows the comparison between the empirical SSR computed at SU station considering TEPT as a reference and the modelled amplification computed at the same surface location along the longitudinal cross-section L. On the other hand, as it regards the SU/FO functions (Fig. 8a, c), the first frequency peak is close to 1Hz both in the measured and in the modelled numerical functions while the higher frequency peaks are underestimated of about 1 Hz by the numerical modelling. In general, the SSR function derived from the numerical simulations are in good agreement with empirical data in the frequency range of main interest (2-8Hz) while at lower frequencies an important misfit remains.

After the reliability of the numerical modelling was verified, 2D amplification functions ($A(f)_x$) were obtained calculating the spectral ratios between the ground motion velocities computed all along the surface of the models and at a reference station that, for each model section, is representative of the outcropping bedrock.

Each cross-section was also modelled considering a homogeneous material, i.e. reproducing only its topographic shape. Fig. 11 illustrates the results for the longitudinal homogeneous cross-section L only; this plot shows that topographic effects cannot be responsible for any amplification. A comparison between Fig. 10 and Fig. 11 shows that seismic amplifications at

the landslide site are very complex and strongly controlled by the geological setting of the slope. For the longitudinal cross-section L, hardly any amplification is observed outside from the landslide area while significant amplifications (up to 2) are observed in the landslide mass at frequencies between 2 and 4 Hz. A significant amplification is also visible in the plateau zone (upslope to the landslide mass), which can be related to the modelled stratigraphy and corresponds to frequencies lower than along the landslide slope. It is worth noticing that the TEPT reference station is located out from the modelled section L (Figs.2b and 7). Along the transversal cross-sections the $A(f)_x$ numerical functions reveal amplification up to 2 in a frequency range that is wider for T3 and T4 sections in comparison to T1 and T2. In details, in the case of T1 and T2 seismic amplifications occur in the range 2 to 4 Hz except on the lateral boundaries of the landslide mass. On the contrary, for sections T3 and T4 the main amplifications occur between 2 and 6.5 Hz and they are more uniformly distributed within the landslide mass. Based on the above reported results and in analogy with the observations of Bard and Bouchon (1985) on sediment-filled valley, it is possible to infer that the wave propagation scheme gradually changes from section T1 to section T4 in relation to a decreasing width/depth ratio. This variation causes the seismic response to change from a 1D resonance complicated by effects due to lateral waves propagation to a properly 2D resonance

.

To further highlight the parameter control on such an amplification pattern, 1D-A(f) soil columns, representing only the soft soil resonance due to the landslide mass layering at given locations, were also modelled. The distribution of the aggravation factor, which is computed by the ratio between the 1D-A(f) and the 2D-A(f) along the cross-section and highlights the

differences between the two models (Semblat and Pecker, 2009), shows that the 1D seismic response is very similar to the 2D one (Fig.16): therefore, also the 2D-$A(f)_x$ is mainly controlled by the impedance contrast between the landslide mass debris and the local substratum (i.e. seismic bedrock). On the edges of back-tilted landslide blocks, seismic amplification effects result at higher-frequencies with respect to the rest of the landslide mass.

5. DISCUSSION

The here obtained results demonstrate that an impedance contrast between the landslide mass and the substratum can induce a very complex and broadband seismic response at the Büyükçekmece landslide site while the topographic amplification effects are negligible. This latter result could be expected because the slope angle of the slope hosting the landslide is very low (only 4°) resulting in low amplifications if any.

These findings are in good agreement with previous studies, demonstrating evidences of peculiar site effects on other hillslopes in case of monitored landslide site or unstable slopes (Burjánek *et al*., 2010; Del Gaudio and Wasowski, 2007; 2011; Galea *et al.*, 2014). More in particular, these studies suggest that directional resonance phenomena can be result from a combination of topographic, lithological and structural factors that act together to re-distribute shaking energy, focusing it on site-specific directions. Based on these evidences, it seems difficult to single out the critical factors controlling local seismic effects in landslide masses. Nevertheless, as also demonstrated for the Büyükçekmece landslide case study, the presence of site response can be revealed through reconnaissance techniques by using recordings of

seismic weak motion and/or ambient noise (Del Gaudio *et al.*, 2014 and references therein). Some case studies highlighted the role of site effect in favoring seismically-induced slope failures, for instance through a "self-excitation" process (Bozzano *et al.*, 2008), which can explain how seismic amplification effects can be responsible for triggering far-field and pre-existing large landslides, that represent outliers with respect to the proposed predictive curves (Keefer, 1984; Rodriguez *et al.*, 1999).

The deformations that can occur within the landslide masses, responsible for their earthquake-induced (re)activation, can result by the aforementioned complex interactions between seismic waves and slope. In this regard, 2D-3D geometrical configurations are necessary to account for these effects (Del Gaudio and Wasowski, 2007; Bourdeau and Havenith, 2008; Danneels et al., 2008, Lenti and Martino, 2013, Gischig et al., 2015). It is worth stressing that the here performed study does not account for possible effects related to incidence angle of the seismic waves below the numerical domain; nevertheless, once the numerical model has been calibrated on the empirical functions, future modelling could be focused on assessing the effects related to the proximity of the landslide area to the NAFZ in terms of both incidence angle and nonlinearity effects. To this aim, a higher number of earthquake recordings will be necessary and the dynamic properties of the involved soils should be defined based on specific laboratory tests. As a future perspective, further studies will be devoted to analyze the expected earthquake-triggered landslide mobility based on the measured and modelled local seismic response of the landslide mass.

6. CONCLUSIONS

The multidisciplinary study at the Büyükçekmece landslide test-site (Turkey) showed that the landslide mass involves sandy and clayey deposits of a local Cenozoic succession as well as buildings and roads. A multiparametric monitoring system was installed on July 2014, including seismic, geotechnical and GPS sensors; one-year records allowed to demonstrate that the landslide has a very slow and continuous westward movement with a displacement rate in the order of 2 cm/month. Preliminary correlations between pore water pressures and rainfalls are evident in a seasonal and monthly time intervals. Based on several performed geophysical investigations, the landslide geometry and dynamic soil properties were derived and used for calibrating a numerical model of the local seismic response in the landslide slope. To this aim, transfer and amplification functions were empirically obtained along both longitudinal and transversal cross-sections by in-hole and surface seismic monitoring, through 45 earthquake collected records. The complex geological setting of the landslide slope was modelled by a finite different code, and the counter slope-tilted blocks composing the landslide mass were reproduced. A reliability test was performed to verify the best fit between the empirical and the numerical functions; based on these results, 2D seismic amplification functions and wave propagation patterns along the slope surface were derived, demonstrating that the local seismic amplification is strongly influenced by the local geological setting. Amplifications up to 2 are expected in the slope at frequencies between 2 and 4 Hz and can be related to the impedance contrast between the Büyükçekmece landslide mass and the local substratum (i.e. seismic bedrock). No significant topographic effects were output by modelling the propagation of seismic waves with a normal incidence. These results will

represent the basis for further numerical models focused on possible effects due to directivity and incidence of the seismic waves as well as on nonlinearity up to plasticity of the landslide mass in case of strong motions, that can be responsible for the Büyükçekmece landslide re-activation.

AKNOWLEDGEMENTS

The authors wish to thank the Municipality of Istanbul for data and logistic support provided; Danilo D'Angiò, Andrea Fantini and Antonella Sacco for their contributions to the processing of monitored data and to the geological mapping; Benoit Peboscq, Ethem Görgün and Mehmet Safa Arslan for their supports for geophysical investigations. The authors also thank the TUBITAK Institute (Scientific and Technological Research Council of Turkey) for the accelerometric data provided at the TEPT station. The study was carried out in the framework of the *MARSite – Marmara Supersite: new directions in seismic hazard assessment through focused Earth observation in the Marmara Supersite* (grant agreement n°: 308417 – 7th Framework Programme), WP6 "Earthquake-induced Landslide Hazard in Marmara (co-ordinator: P. Bigarrè). The Authors thank H.B. Havenith and other two anonymous reviewers for their useful suggestions.

REFERENCES

Alfaro, P., Delgado, J., Garcia-Tortosa, F.J., Giner, J.J., Lenti, L., Lopez-Casado, C., Martino, S., Scarascia Mugnozza, G., 2012. The role of near-field interaction between seismic waves and slope on the triggering of a rockslide at Lorca (SE Spain). *Natural Hazards and Earth System Sciences*, 3631-3643, ISSN: 1561-8633.

Bard, P.Y., Bouchon, M., 1985. The two-dimensional resonance of sediment-filled valleys, Bull. Seismol. Soc. Am., 75, 519–541.

Bird, J.F., Bommer, J.J., 2004. Earthquake losses due to ground failure. Engineering Geology, 75, 147–179.

Borcherdt, R.D., 1994. Estimates of site-dependent response spectra for design (methodology and justification), Earthquake Spectra, 10, 617–653.

Bourdeau, C., Havenith, H.B., 2008. Site effects modeling applied to the slope affected by the Suusamyr earthquake (Kyrgyzstan, 1992). Engineering Geology, 97, 126-145.

Bozzano, F., Lenti, L., Martino, S., Paciello, A., Scarascia Mugnozza, G., 2008. Self-excitation process due to local seismic amplification responsible for the reactivation of the Salcito landslide (Italy) on 31 October 2002 Journal of Geophysical Research, 113, B10312.

Bozzano, F., Lenti, L., Martino, S., Paciello, A., Scarascia Mugnozza, G., 2011. Evidences of landslide earthquake triggering due to self-excitation process. International Journal of

Earth Sciences 100, 861-879.

Burjánek, J., Gassner-Stamm, G., Poggi, V., Moore, J.R., Fäh, D., 2010. Ambient vibration analysis of an unstable mountain slope. Geophys. J. Int. 180, 820–828.

Bray, J.D., Rathje, E.M., 1998. Earthquake-induced displacements of solid-waste landfills. J. Geotech. and Geoenvir. Engrg., ASCE, 124(3), 242–253.

Coccia, S., Del Gaudio, V., Venisti, N., Wasowski J., 2010. Application of Refraction Microtremor (ReMi) technique for determination of 1-D shear wave velocity in a landslide area. Journal of Applied Geophysics, 21 (2-3), 71-89.

Cruden, D.M., Varnes, D.J., 1996. Landslide types and processes, in Landslides: Investigation and Mitigation, A. K. Turner and R. L. Schuster (Editors), Transportation Research Board, Spec. Report 247, National Research Council, National Academy Press, Washington, DC, 36–75.

Cundal, P., Hansteen, E., Lacasse, S., Selnes P.B., 1980. "NESSI, Soil Structure Interaction Program for Dynamic and Static Problems", Norges Geotekniske Institute, Norway, Report 51508-9.

Dalgiç, S., 2004. Factors affecting the greater damage in the Avcılar area of Istanbul during the 17 August 1999 Izmit earthquake. Bull. Eng. Geol. Env., 63, 221–232.

Danneels, G., Bourdeau, C., Torgoev, I., Havenith, H.B., 2008. Geophysical investigation and dynamic modeling of unstable slopes: case-study of Kainama (Kyrgyzstan). Geophysical Journal International, 175(1), 17–34.

Del Gaudio, V., Muscillo, S., Wasowski, J, 2014. What we can learn about slope response to earthquakes from ambient noise analysis: An overview. Eng. Geol., 182, 182-200.

Del Gaudio, V., Wasowski, J., 2007. Directivity of slope dynamic response to seismic shaking. Geophys. Res. Lett 34, L12301, doi:10.1029/2007GL029842.

Del Gaudio, V., Wasowski, J., 2011. Advances and problems in understanding the seismic response of potentially unstable slopes. Eng. Geol., 122, 73-83.

Delgado, J., Garrido, J., López-Casado, C., Martino, S., Peláez, J.A., 2011. On far field occurrence of seismically induced landslides. Engineering Geology, 123, 204-213.

Delgado, J., Garrido, J., Lenti, L., Lopez-Casado, C., Martino, S., Sierra, F.J., 2015. Unconventional pseudostatic stability analysis of the Diezma landslide (Granada, Spain) based on a high-resolution engineering-geological model. Engineering Geology, 184, 81-95.

Dilley, M., Chen, R.S., Deichmann, U., Lerner-Lam, A.L., Arnold, M., Agwe, J. Buys, P., Kjekstad, O., Lyon, B., Yetman, G., 2005. Natural disaster hotspots: a global risk analysis. The World Bank Hazard Management Unit, Washington.

Field, E.H., Jacob, K., 1995. A comparison and test of various site response estimation techniques, including three that are not reference-site dependent, Bull. Seism. Soc. Am., 85, 1127–1143.

Galea, P., D'Amico, S., Farrugia, D., 2014. Dynamic characteristics of an active coastal spreading area using ambient noise measurements - Anchor Bay, Malta. Geophys. J. Int., 199, 1166–1175.

Gischig, V.S., Eberhardt, E., Moore, J.R., Hungr, O., 2015. On the seismic response of deep-seated rock slope instabilities - Insights from numerical modeling. Eng. Geol., 193, 1-18.

Haque, U., Blum, P. , da Silva, P.F., Andersen, P., Pilz, J., Chalov, S.R., Malet, J.P., Auflič, M.J., Andres, N., Poyiadji, E., Lamas, P.C., Zhang, W., Peshevski, I., Pétursson, H.G., Kurt, T., Dobrev, N., García-Davalillo, J.C., Halkia, M., Ferri, S., Gaprindashvili, G., Engström, J., Keellings, D., 2016. Fatal landslides in Europe. Landslides, DOI 10.1007/s10346-016-0689-3.

ITASCA, 2011." FLAC 7.0: User manual", Licence number SN 213-33-760- clé 29753, IFSTTAR.

Keefer, D.K., 1984. Landslides caused by earthquakes. Geol. Soc. Am. Bull., 95, 406-421.

Kuhlemeyer, R.L., Lysmer, J., 1973. Finite element method accuracy for wave propagation problems, J. Soil Mech. Found. Eng., Div. ASCE 1973, 99(SM5), 421-427.

Lenti, L., Martino, S., 2012. The interaction of seismic waves with step-like slopes and its influence on landslide movements. Engineering Geology, 126, 19-36.

Lenti, L., Martino, S., 2013. A Parametric Numerical Study of Interaction between seismic waves and landslides for the evaluation of the susceptibility to seismically induced displacements. Bull. Seism. Soc. Am., 103(1), 33-56.

Lenti, L., Martino, S., Musolino G., 2016. Considering seismic coefficient distributions within slopes to calculate landslide reactivation probability. Bull. Eng. Geol. Env., doi: 10.1007/s10064-016-0938-7

Martino, S., 2015. Earthquake-induced reactivation of landslides: recent advances and future perspectives. In: Sebastiano D'Amico. Earthquakes and Their Impact on Society. p. 291-322, Springer International Publishing AG Switzerland, ISBN: 978-3-319-21752-9, doi: 10.1007/978-3-319-21753-6_10.

Martino, S., Lenti, L., Delgado, J., Garrido, J., Lopez-Casado, C., 2016. Application of a

characteristic periods-based (CPB) approach to estimate earthquake-induced displacements of landslides through dynamic numerical modelling. Geophys. J. Int., 206, 85–102.

Méric O., Garambois S., Malet J.P., Cadet H., Guéguen P., Jongmans D., 2007. Seismic noise-based methods for soft-rock landslide characterization. Bull. Soc. Géol. Fr., 178(2), 137–148.

Petley, D., 2012. Global patterns of loss of life from landslides. Geology 40(10): 927–930.

Rodriguez, C.E., Bommer, J.J., Chandler, R.J., 1999. Earthquake-induced landslides: 1980-1997. Soil Dynamic Earthquake Engineering, 18, 325-346.

Semblat, J.F., Pecker, A., 2009. "Waves and vibration in soils: Earthquakes, Traffic, Shocks, Construction works", IUSS Press, Pavia (Italy), p. 499.

Sen, S., 2007. A fault zone cause of large amplification and damage in Avcılar (west of Istanbul) during 1999 Izmit earthquake. Nat. Hazards, 43, 351–363.

Varnes, D.J., 1978. Slope movement types and processes. In: Schuster R.L. and Krizek R.J. (Eds.), Special Report 176 Landslides: Analysis and Control. Transportation Research Board, National Research Council, Washington D.C., 11-33.

Yalcinkaya, E., Alp, H., Ozel, O., Gorgun, E., Martino, S., Lenti, L., Bourdeau, C., Bigarre, P., Coccia, S, 2016. Near-surface geophysical methods for investigating the Buyukcekmece landslide in Istanbul, Turkey. Journal of Applied Geophysics 134, 23–35.

CAPTION TO FIGURES AND TABLES

Fig. 1 – Sea of Marmara region (up) and zoom on the Avcilar-Beylikdüzü peninsula (down). The location of the Büyükçekmece landslide and the epicenters of the 45 earthquakes recorded during 2015 at SU, FO and TEPT seismic stations (see Table 1 for a description of these earthquakes and Fig.2 for the location of the seismic stations) are also shown (in red the earthquake used for the numerical modelling).

Fig. 2 – Geological (a) and geomorphological (b) maps of the Büyükçekmece landslide: 1) alluvial and coastal deposits (Holocene); 2) silty-clays of the Danisment Formation (upper Oligocene); 3) clays with tuffs for the Danisment Formation (upper Oligocene-lower Miocene); 4) sands and gravels of the Istanbul Formation - Kiraç member (upper Oligocene- lower Miocene); 5) calcarenites of the Çekmece Formation - Bakirköy member (upper Miocene); 6) earthflow debris; 7) rototranslational landslide mass; 8) slope debris; 9) landslide counterslope tilted terrace; 10) rototranslational landslide scarp; 11) earthflow crown; 12) fault; 13) seismic lines; 14) noise measurement station; 15) VES measurement point; 16) accelerometric station of the KOERI (Kandilli Observatory and Earthquake Research Institute); 17) monitoring stations installed during the MARSite project: (SC) stands for “Shopping center”, FM for “Farm” and HS for “House”. SU and FO accelerometric stations are in the FM location.

Fig. 3 – Geological units outcropping in the landslide area: a) claystones of the Danisment Formation (upper Oligocene); b) silty-clay with tuff levels in the Danisment Formation

(upper Oligocene); c) sands and gravels belonging to the Kiraç member of the Istanbul Formation (Upper Oligocene – Lower Miocene); d) calcarenites and marls belonging to the Bakirköy member of the Çekmece Formation (upper Miocene); e) panoramic photo-view of the Büyükçekmece landslide detachment area (location of the accelerometric stations SU, FO, TEPT is also shown).

Fig. 4 – Geological cross-sections constructed along the traces L, T1, T2, T3 and T4 of Fig.3. See Fig.3 for the legend.

Fig. 5 – Monitored parameters at FM station: u(t) rate of water pore pressures (black dots and grey triangles); cumulative rainfall (black line), cumulative Arias intensity (AI), GPS displacement WE component). Dashed lines envelope the seasonal trend; while the values above the line can be regarded as out-of-trend.

Fig. 6 – Arias intensity (AI) vs. peak of ground acceleration (PGA) and characteristic period of the earthquake(Tm) vs. AI distributions for the 45 earthquakes recorded during 2015 at SU, FO and TEPT stations. The WE ad NS horizontal components are shown.

Fig. 7 – a) average HVSR (continuous line) ± standard deviation (dashed lines) obtained for the earthquakes recorded during 2015 at TEPT station; b) SSRs (computed as SU/TEPT spectral ratio) for EQ22, EQ33 and EQ37 compared with the standard deviations (dashed black lines) of the SSRs computed for the 45 recorded earthquakes of Table 1.

Fig.8 – Cross-section L: a) numerical SSR (red, blue, green and cyan lines for Ricker input, EQ22, EQ33 and EQ37, respectively) obtained at station SU compared to FO. The

empirical average SSR (black) from the 45 earthquakes (WE ground-motion component) and the related standard deviation (black dashed lines) are also shown; b) empirical average SSR (black) obtained at station SU compared to TEPT and numerical SSR (red) obtained at the same location in the model by considering a Ricker seismic input signal. Cross section T1: c) numerical SSR (red, blue, green and cyan lines for Ricker input, EQ22, EQ33 and EQ37 respectively) obtained at station SU compared to FO. The empirical average SSR (black) from the 45 earthquakes (NS ground-motion component) and the related standard deviation (black dashed lines) are also shown.

Fig. 9 – Time histories recorded at the TEPT station (only the WE component is shown) considered for the modeling (left column) and related FFT (right column). From top to bottom: a) Richer input, b) EQ22, c) EQ33, d) EQ37.

Fig.10 - Propagation (Ricker wavelet) along the longitudinal cross-section L as revealed by displacements histories versus time (top), amplification function ($A(f)_x$) (middle) and model considered (heterogeneous filling within the landslide mass) (bottom): 1) claystones; 2) sands and gravels; 3) calcarenites and marls; 4) slope debris; 5) sliding surfaces; 6) fault.

Fig.11 - Propagation (Ricker wavelet) along the longitudinal cross-section L as revealed by displacements histories versus time (top), amplification function ($A(f)_x$) (middle) and model considered (homogeneous model). Key to legend: 1) claystones (bottom).

Fig.12 - Propagation (Ricker wavelet) along the transversal cross-section T1 as revealed by displacements histories versus time (top), amplification function ($A(f)_x$) (middle) and

model considered (heterogeneous filling within the landslide mass) (bottom). Key to legend: 1) claystones; 2) sands and gravels; 3) calcarenites and marls; 4) slope debris; 5) sliding surfaces; 6) fault.

Fig.13 - Propagation (Ricker wavelet) along the transversal cross-section T2 as revealed by displacements histories versus time (top), amplification function ($A(f)_x$) (middle) and model considered (heterogeneous filling within the landslide mass) (bottom). Key to legend: 1) claystones; 2) sands and gravels; 3) calcarenites and marls; 4) slope debris; 5) sliding surfaces; 6) fault.

Fig.14 - Propagation (Ricker wavelet) along the transversal cross-section T3 as revealed by displacements histories versus time (top), amplification function ($A(f)_x$) (middle) and model considered (heterogeneous filling within the landslide mass) (bottom). Key to legend: 1) claystones; 2) sands and gravels; 3) calcarenites and marls; 4) slope debris; 5) sliding surfaces; 6) fault.

Fig.15 - Propagation (Ricker wavelet) along the transversal cross-section T4 as revealed by displacements histories versus time (top), amplification function ($A(f)_x$) (middle) and model considered (heterogeneous filling within the landslide mass) (bottom). Key to legend: 1) claystones; 2) sands and gravels; 3) calcarenites and marls; 4) slope debris; 5) sliding surfaces; 6) fault.

Fig. 16 – Aggravation factor computed by the ratio between the 1D-A(f) and the 2D-A(f) along the longitudinal cross section L. Key to legend: 1) claystones; 2) sands and gravels; 3) calcarenites and marls; 4) slope debris; 5) sliding surfaces; 6) fault.

Table 1 - Earthquakes recorded at MARSite and TEPT (KOERI) stations from October 2014 to May 2015, during the project (see Fig.1 for epicenter location).

Table 2 - Physical parameters of the Büyükçekmece landslide. The geotechnical units are derived from field measurements and literature

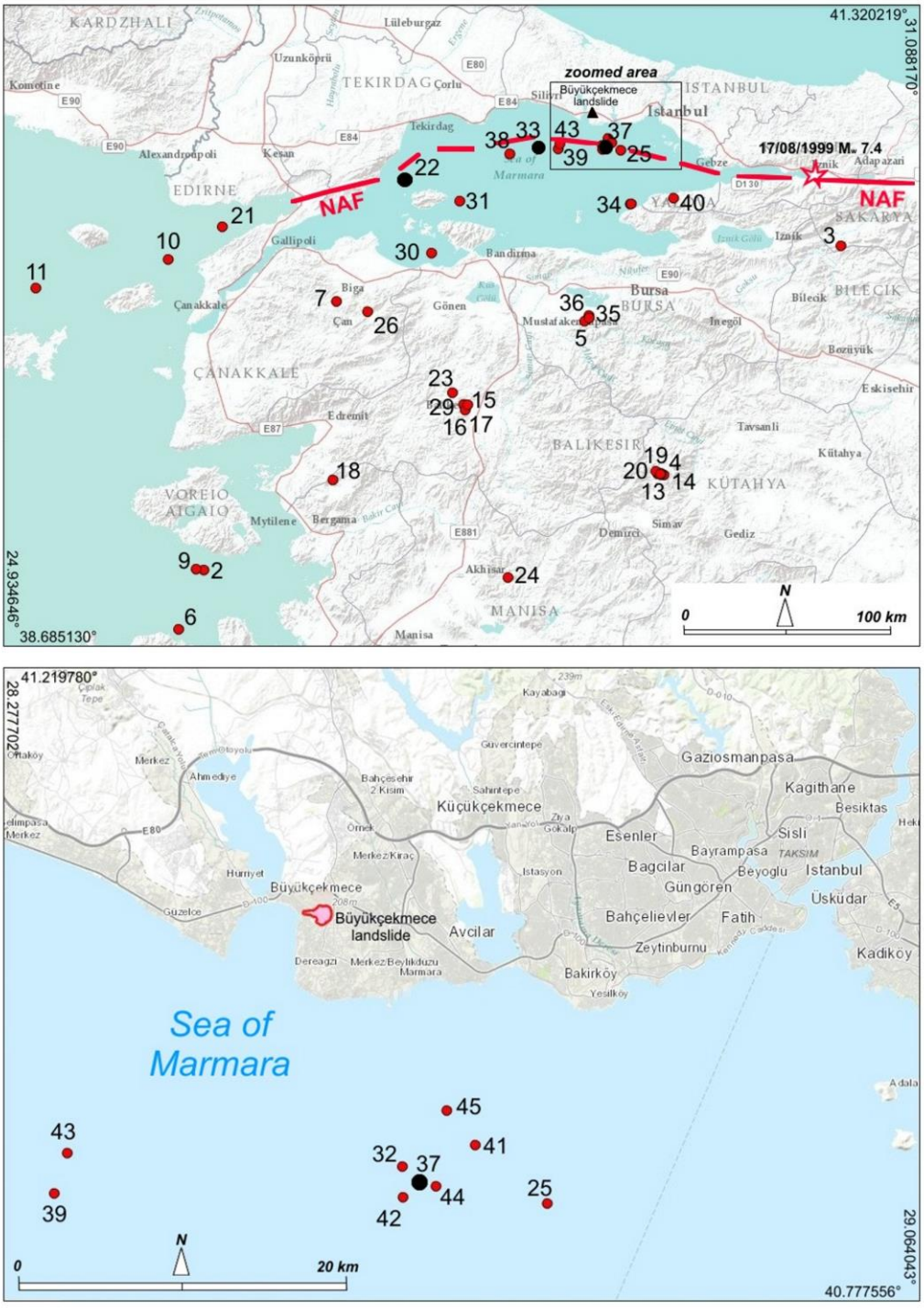

Figure 1

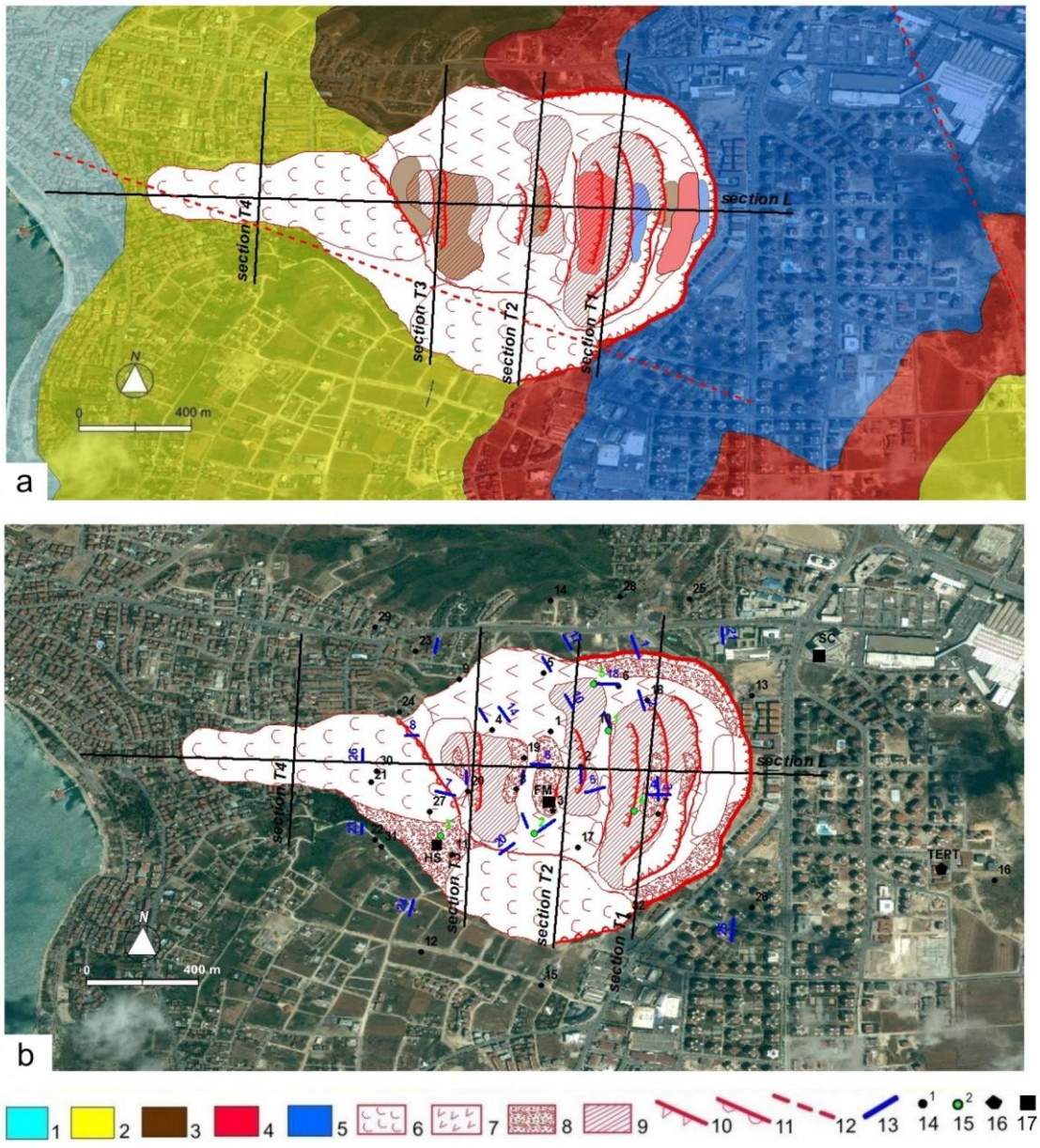
section T4
section T3
section T2
section T1
section L
N
0
400 m
a
SC
FM
HS
TEPT
b
1
2
3
4
5
6
7
8
9
10
11
12
13
14
15
16
17

Figure 2

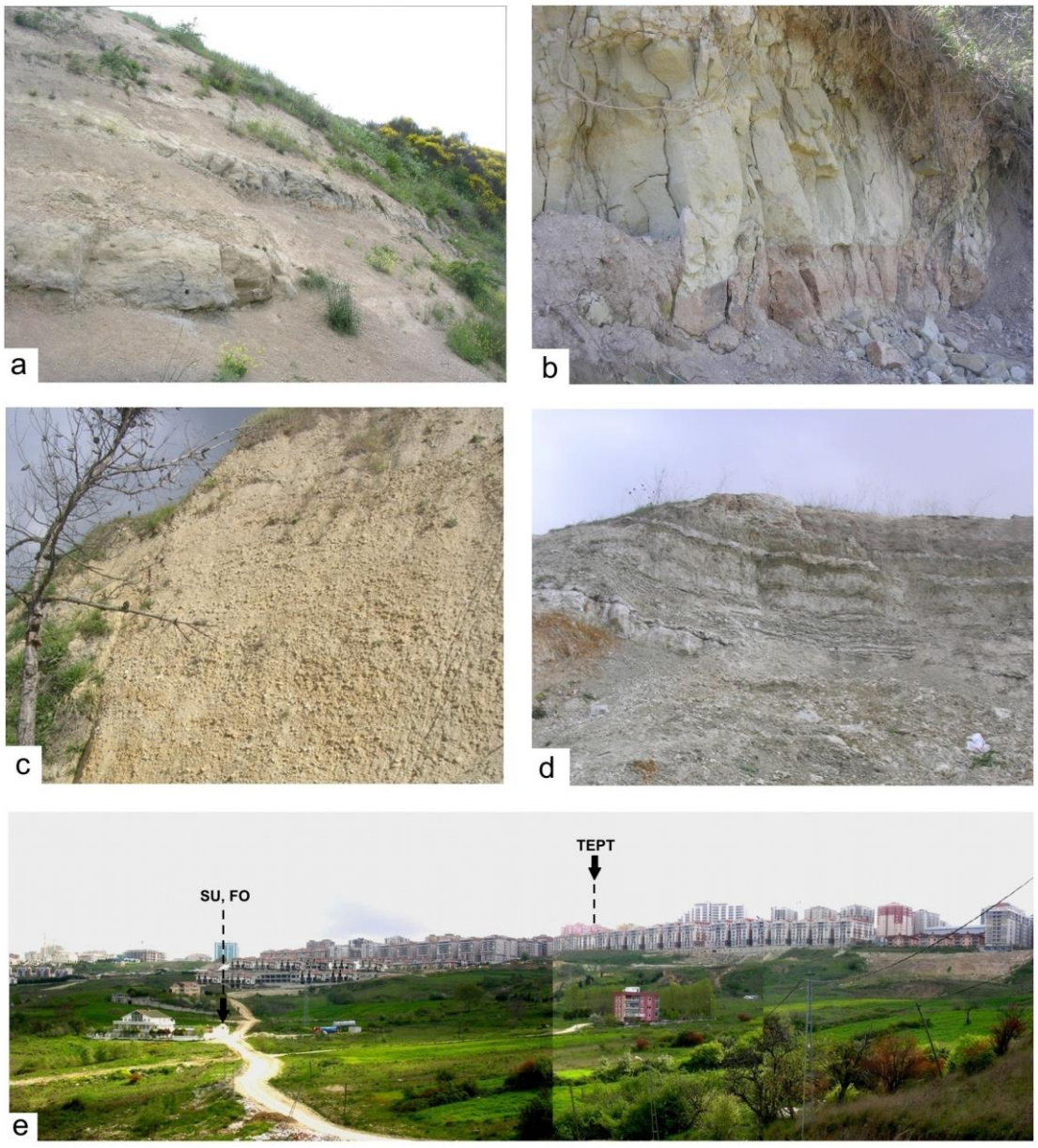

Figure 3

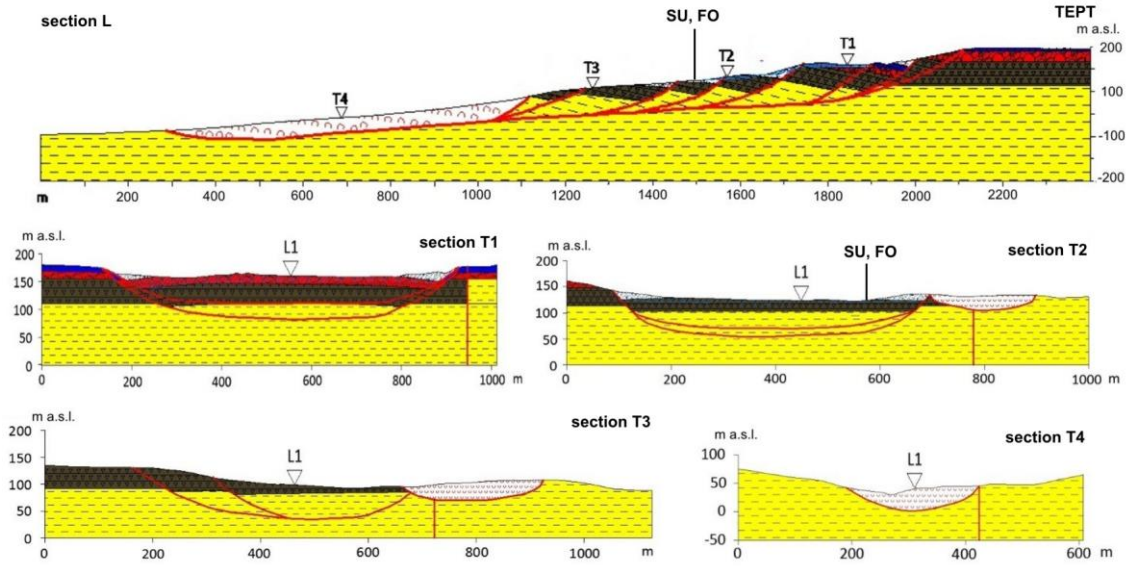

Figure 4

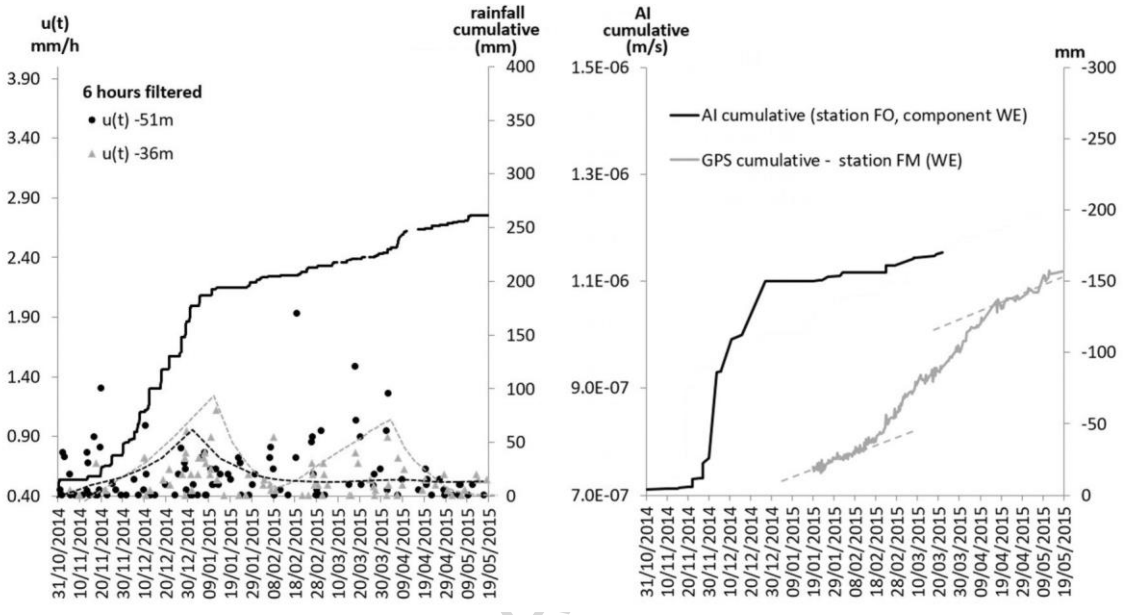

Figure 5

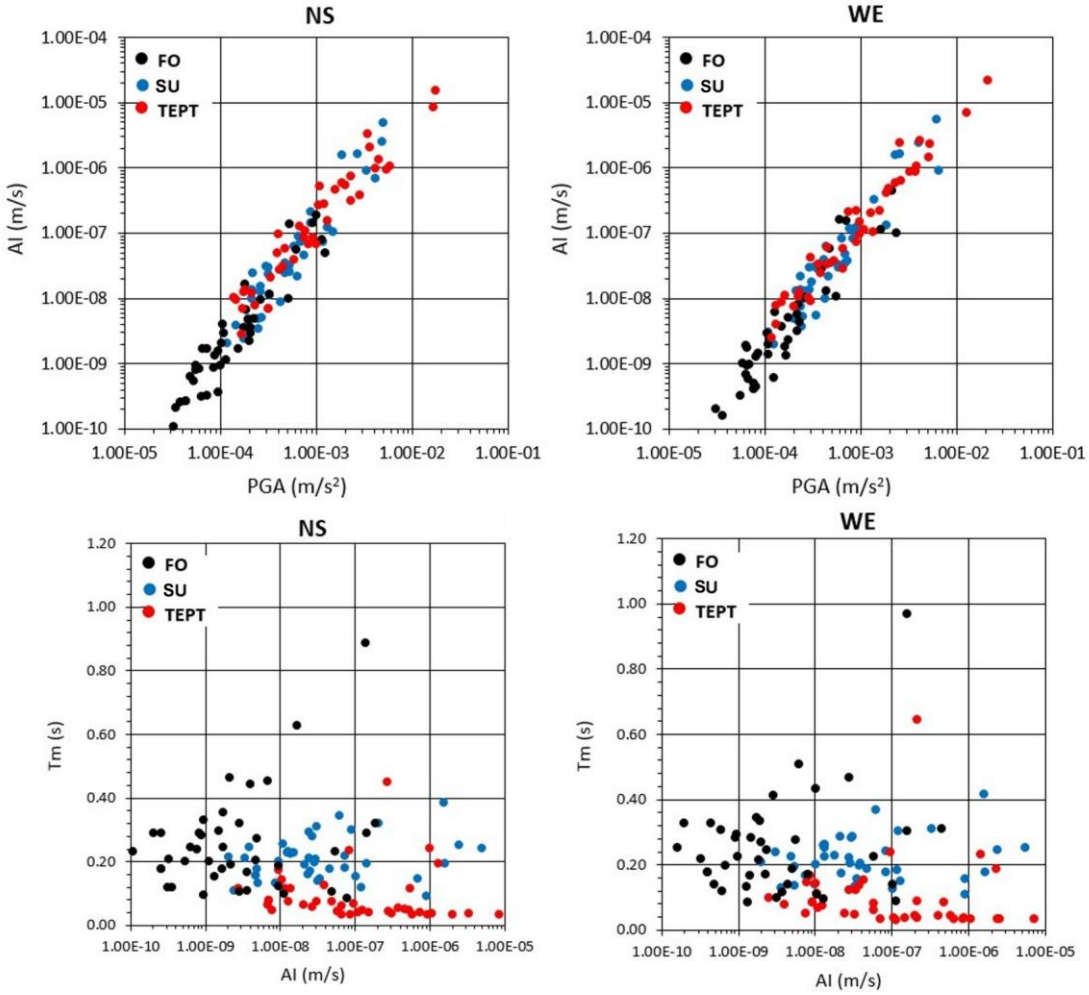

Figure 6

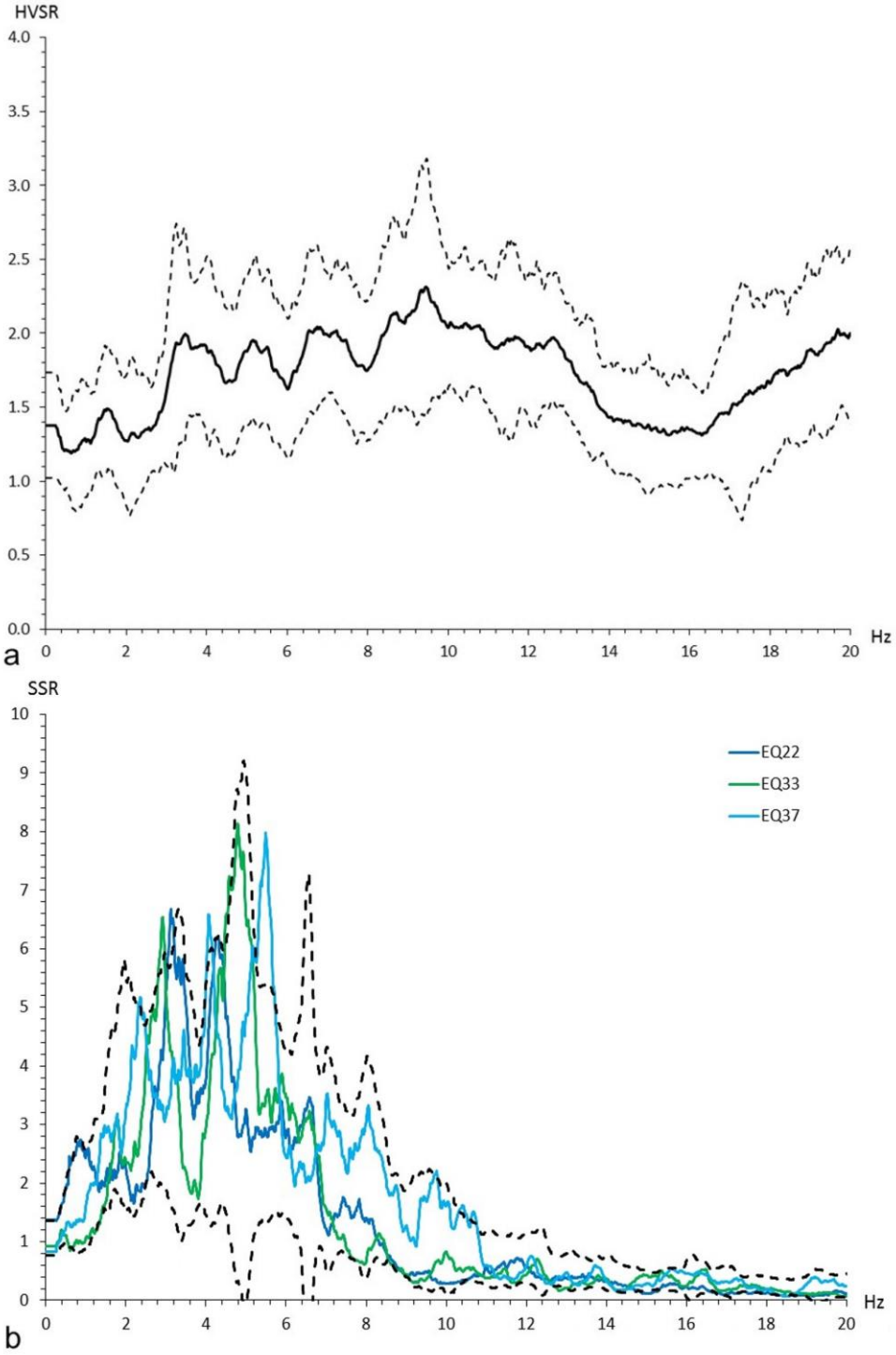

Figure 7

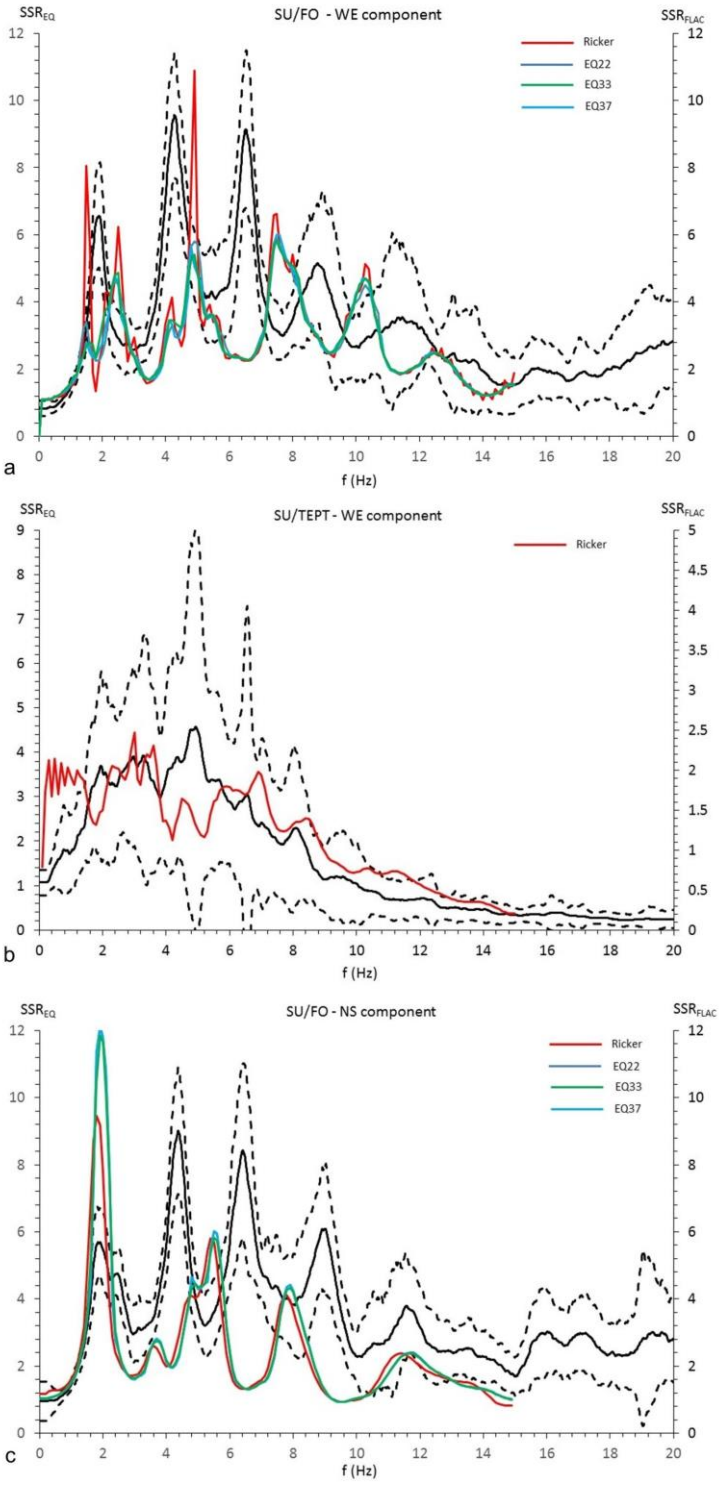

Figure 8

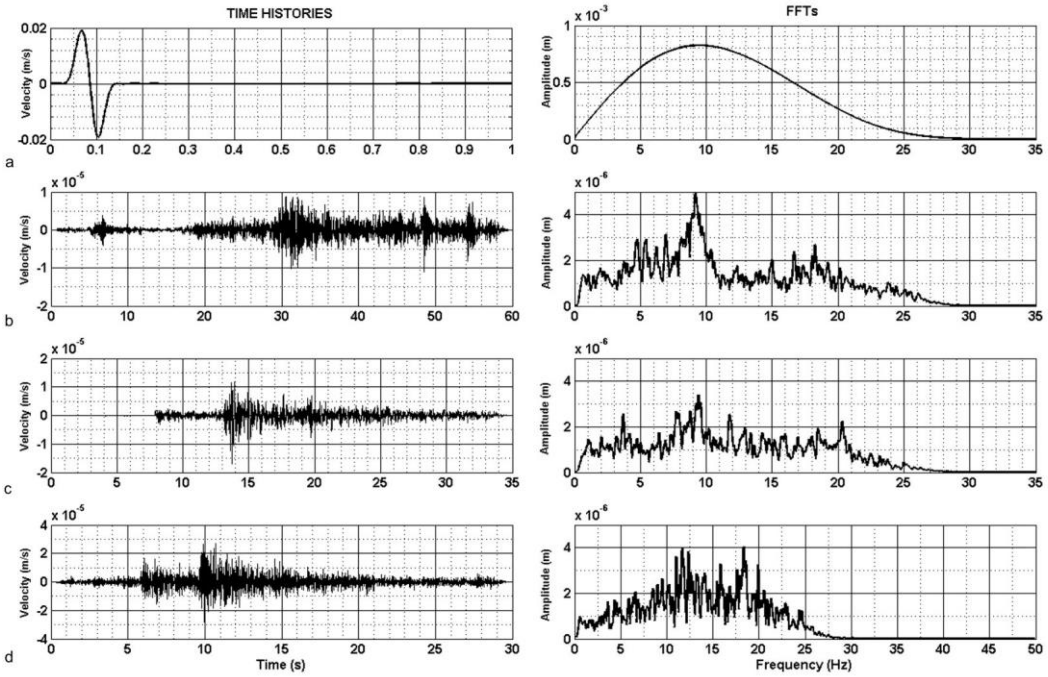

Figure 9

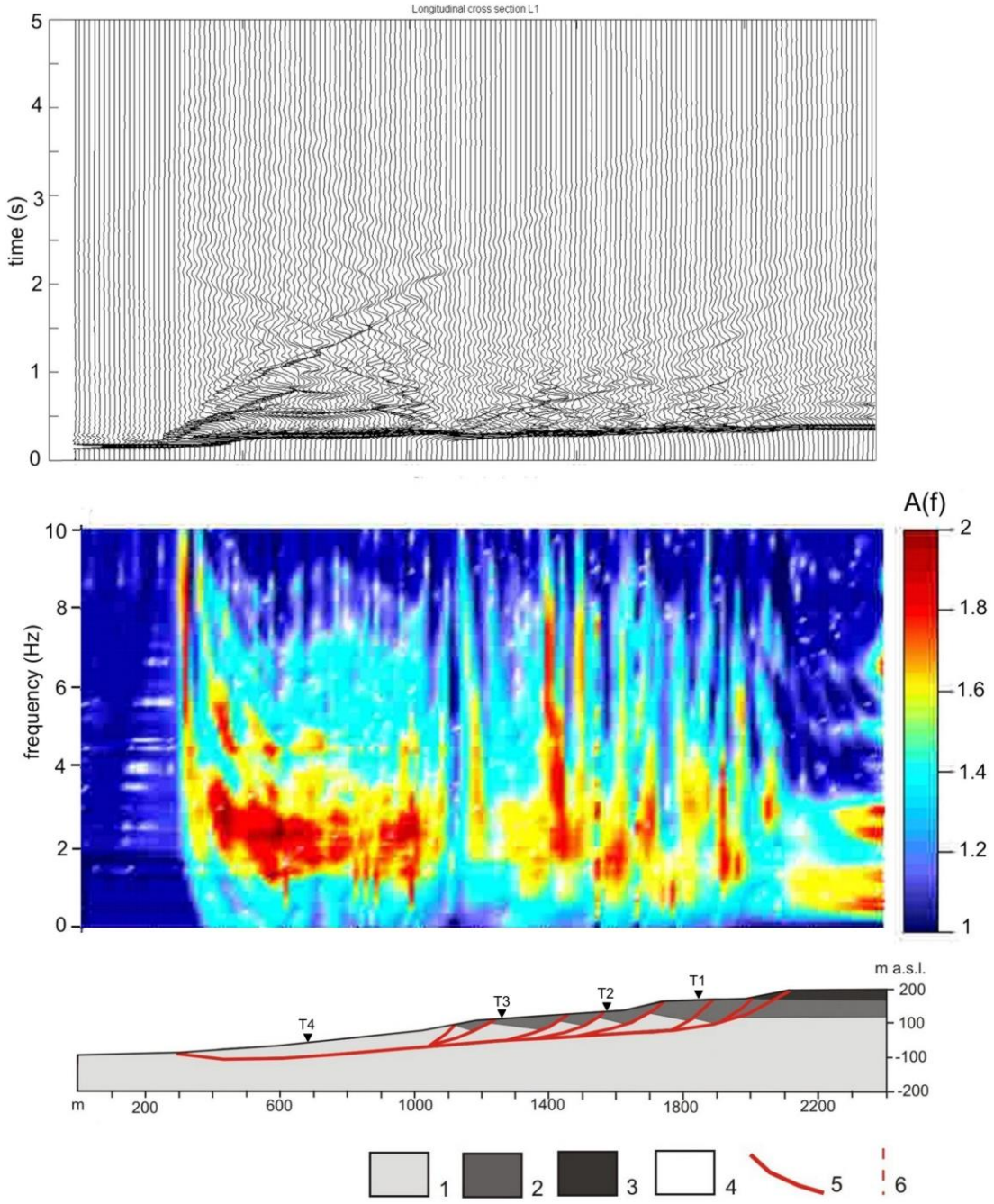
Longitudinal cross section L1
time (s)
frequency (Hz)
A(f)
m a.s.l.
T1
T2
T3
T4
m
200
600
1000
1400
1800
2200
1
2
3
4
5
6

Figure 10

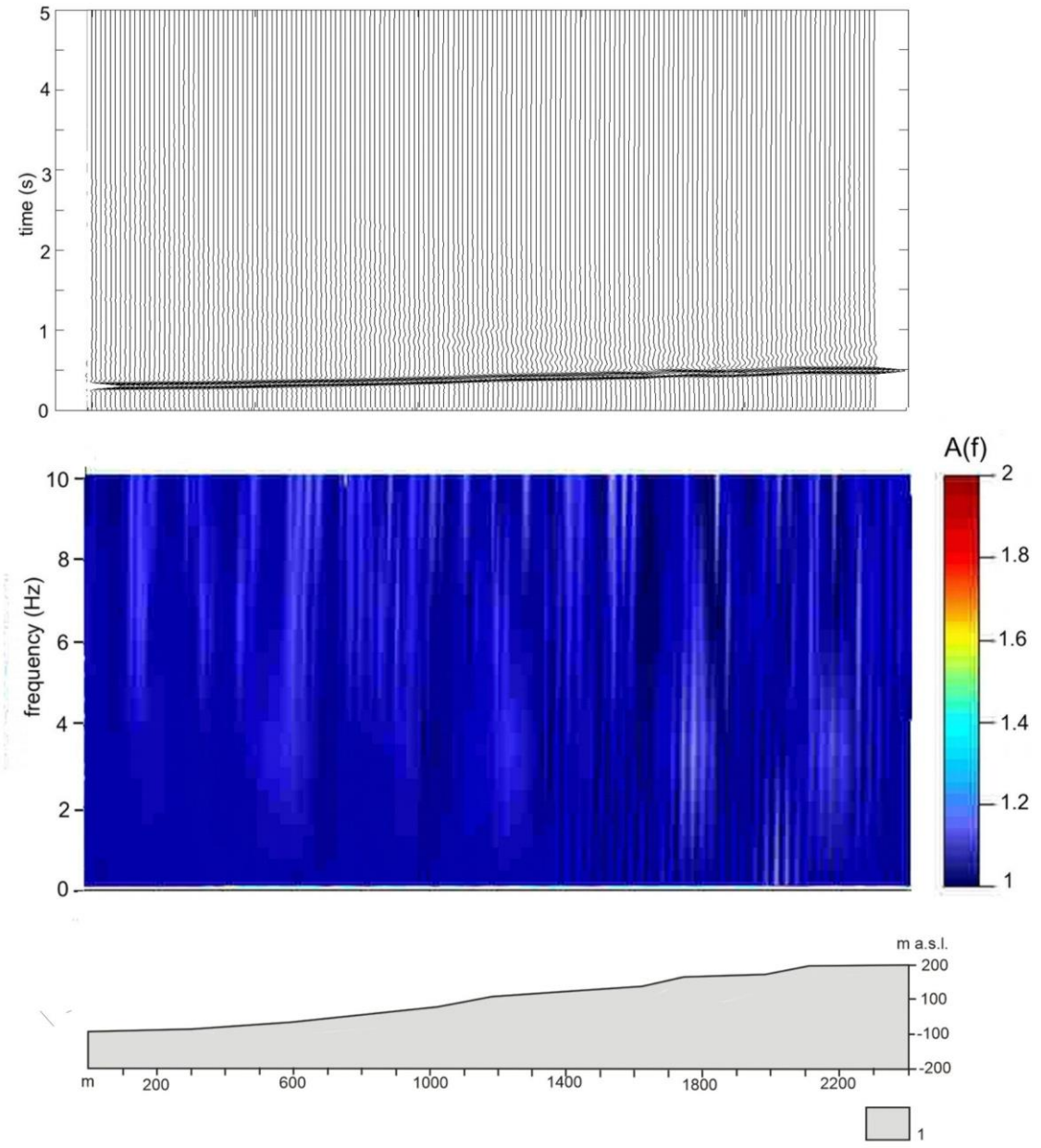

Figure 11

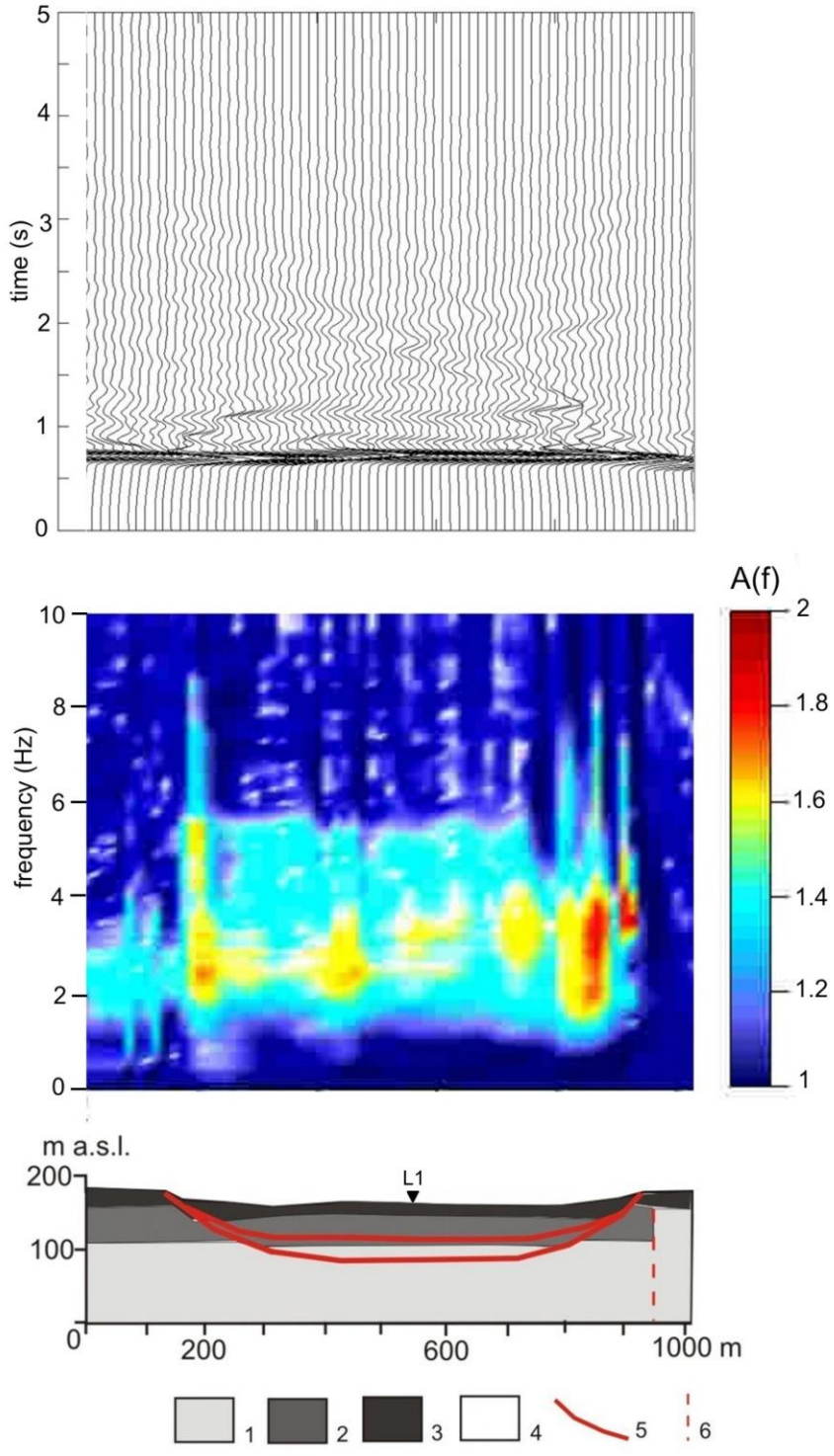

Figure 12

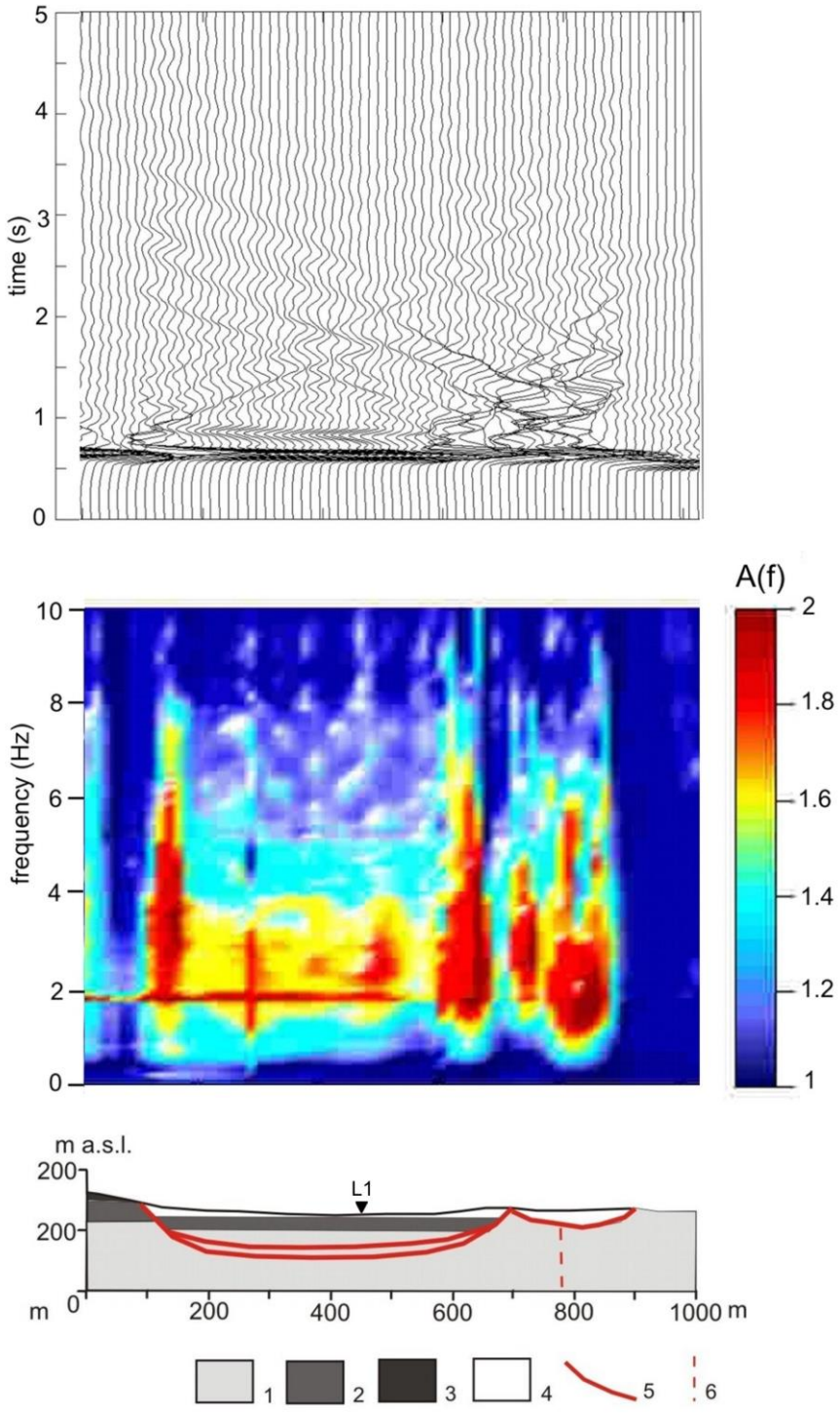

Figure 13

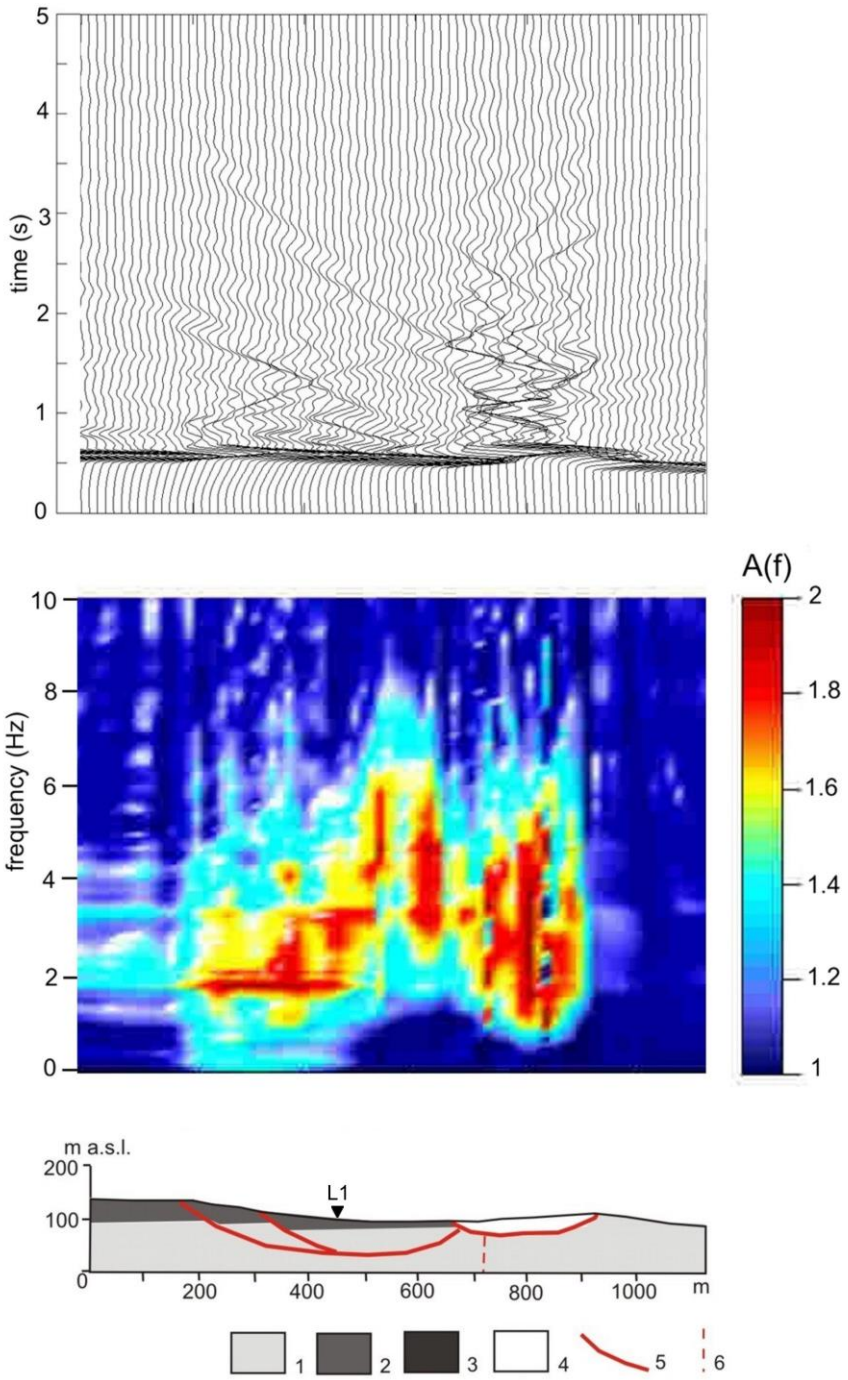

Figure 14

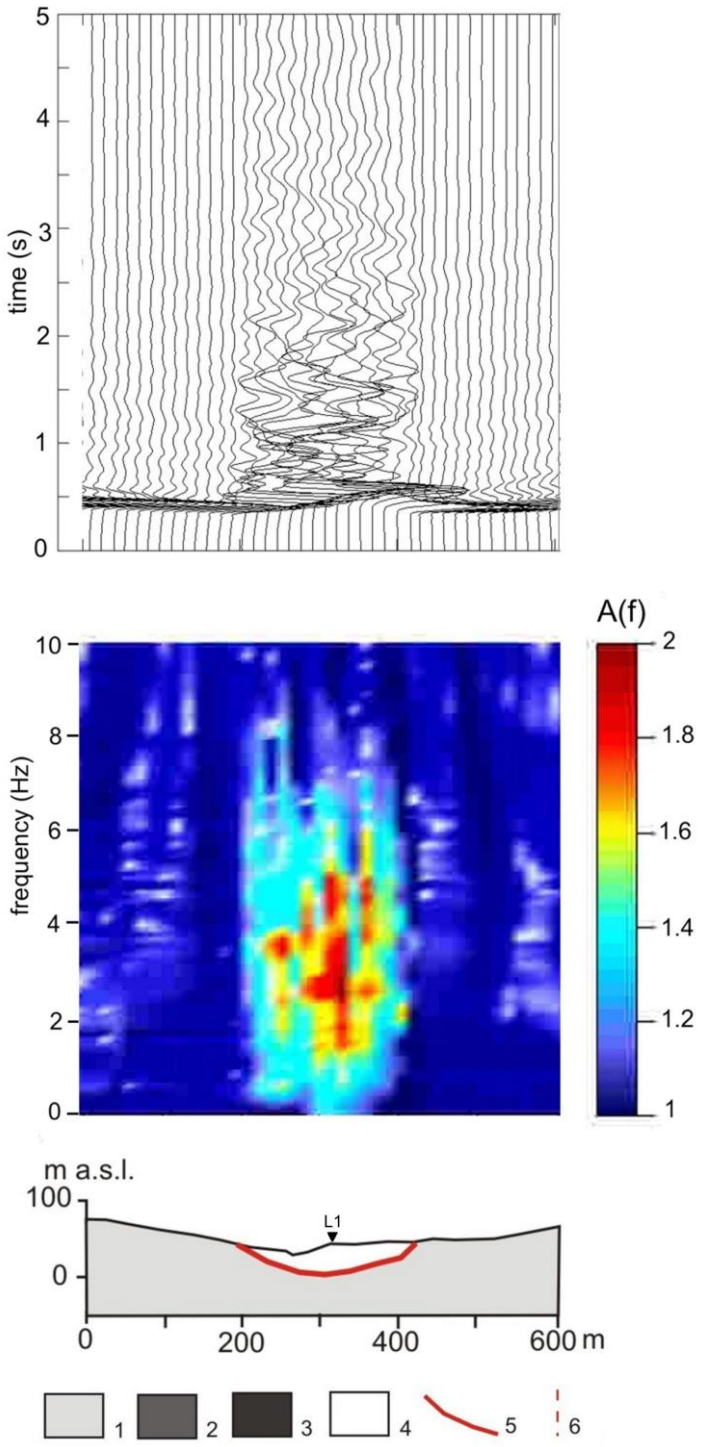

Figure 15

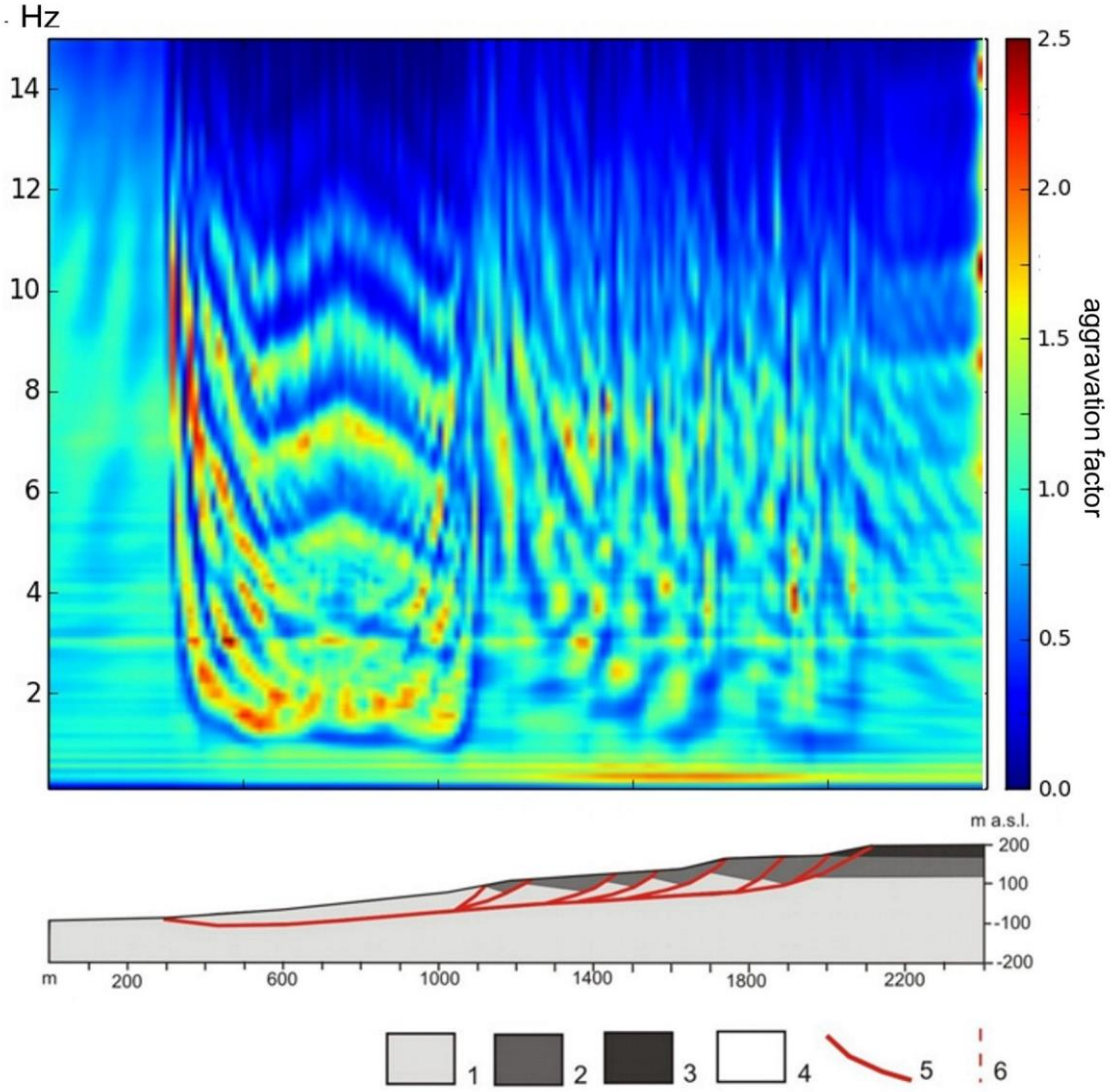

Figure 16

Table 1

#	Time (dd/mm/yyyy)	Epicentral Location	Lat	Long	M
EQ1	11/22/2014	ROMANYA	45.742	27.2147	5.6
EQ2	12/6/2014	AEGEAN SEA	38.8942	26.2723	5.1
EQ3	10/22/2014	PAMUKOVA	40.4047	30.1188	4.5
EQ4	11/28/2014	SIMAV (KUTAHYA)	39.3512	29.018	4.5
EQ5	1/23/2015	UGURLUPINAR-MUSTAFAKEMALPASA (BURSA)	40.0647	28.587	4.5
EQ6	12/4/2014	SAKIZADASI (AEGEAN SEA)	38.6145	26.1205	4.4
EQ7	12/16/2014	CELTIK-BIGA (CANAKKALE)	40.1478	27.0735	4.4
EQ8	11/26/2014	SUDOSEGI-SIMAV	39.3408	29.0512	4.1
EQ9	12/6/2014	AEGEAN SEA	38.899	26.2262	4.1
EQ10	2/2/2015	SAROS KORFEZI (AEGEAN SEA)	40.3412	26.0567	4.1
EQ11	11/27/2014	AEGEAN SEA	40.2098	25.2578	4.0
EQ12	11/30/2014	SIMAV (KUTAHYA)	39.3487	29.0332	3.9
EQ13	11/15/2014	SIMAV	39.3422	29.032	3.8
EQ14	11/16/2014	SIMAV	39.3468	29.0128	3.8
EQ15	2/23/2015	KABAKDERE-(BALIKESIR)	39.663	27.8603	3.8
EQ16	3/19/2015	KABAKDERE-(BALIKESIR)	39.6697	27.8405	3.8
EQ17	3/18/2015	BALIKESIR	39.644	27.8502	3.7
EQ18	11/22/2014	BERGAMA (IZMIR)	39.3172	27.0518	3.6
EQ19	11/26/2014	SIMAV	39.3575	29.0008	3.5
EQ20	11/27/2014	SIMAV (KUTAHYA)	39.3448	29.0292	3.5
EQ21	12/6/2014	SAROSKORFEZI (AEGEAN SEA)	40.4917	26.3838	3.5
EQ22	2/1/2015	GUZELKOY ACIKLARI-TEKIRDAG (MARMARA SEA)	40.7125	27.4973	3.5
EQ23	2/27/2015	AKTARMA-(BALIKESIR)	39.7248	27.7733	3.4
EQ24	11/27/2014	GORDES (MANISA)	38.8595	28.1088	3.3
EQ25	11/10/2014	MARMARA SEA	40.8433	28.7897	3.2
EQ26	11/20/2014	KAYNARCA-BIGA	40.1008	27.2618	3.2
EQ27	12/16/2014	ARMUTLU (YALOVA)	40.596	28.848	3.2
EQ28	1/26/2015	SOGUTALAN-MUSTAFAKEMALPASA (BURSA)	40.0558	28.571	3.2
EQ29	2/23/2015	KABAKDERE-(BALIKESIR)	39.6688	27.8653	3.2
EQ30	3/8/2015	ERDEK KORFEZI (MARMARA SEA)	40.3705	27.6472	3.2
EQ31	3/31/2015	ERDEK ACIKLARI-BALIKESIR (MARMARA SEA)	40.6097	27.817	3.1
EQ32	1/19/2015	MARMARA SEA	40.8648	28.6787	3.0
EQ33	11/22/2014	MARMARA SEA	40.8545	28.2947	2.9
EQ34	12/11/2014	ESENKOY-CINARCIK (YALOVA)	40.5978	28.8527	2.9
EQ35	1/24/2015	INCEALIPINAR-MUSTAFAKEMALPASA (BURSA)	40.0827	28.5975	2.9
EQ36	1/23/2015	INCEALIPINAR-MUSTAFAKEMALPASA (BURSA)	40.0707	28.5985	2.8

EQ37	3/8/2015	MARMARA SEA	40.8565	28.6922	2.8
EQ38	11/21/2014	MARMARA SEA	40.8262	28.119	2.7
EQ39	2/23/2015	MARMARA SEA	40.8492	28.4123	2.6
EQ40	1/22/2015	CINARCIK (YALOVA)	40.6233	29.1082	2.5
EQ41	3/8/2015	AVCILAR (ISTANBUL)	40.8772	28.7345	2.4
EQ42	3/22/2015	MARMARA SEA	40.847	28.6792	2.4
EQ43	2/23/2015	MARMARA SEA	40.8725	28.4223	2.3
EQ44	3/9/2015	MARMARA SEA	40.8533	28.7045	2.0
EQ45	12/27/2014	AVCILAR (ISTANBUL)	40.8972	28.7128	1.9

Table 2

Geotechnical Unit	Vs (m/s)	Vp (m/s)	Density (kg/m^3)
Earth-flows debris	148	259	1800
Debris	156 - 183	273 – 321 in dry zones	1800
		1079 – 1306 in wet zones	
Calcarenites	190 – 255	334 - 445	2400
Sands and gravels	203 - 270	357 – 476 in dry zones	1800
		1600 in wet zones	
Clays with tuffs	226 - 373	397 – 656 in dry zones	2000
		1571 - 2000 in wet zones	
Silty-clays	366 - 452 in the landslide mass	642 – 793 in the landslide mass	2100
	600 - 1000 in the substratum	1052 - 1757 in the substratum	

Highlights

Results of earthquake measurements performed for obtaining local seismic response in a landslide area.

In hole and surface measurements were used and compared.

A numerical modelling was based on a detailed engineering-geological reconstruction of the landslide slope.

Local seismic amplification resulted for the landslide mass.

.